EFFECT OF TEMPERATURE RATIO (T_S/T_M) AND TIME ON THE SINTERING BEHAVIOR OF METALLIC 316L STAINLESS STEEL COUPONS COUPONS PRODUCED USING JET-BINDER TECHNOLOGY

by

Hsiang-Ling Juan

B.S., National Chung Hsing University, 2014

Submitted to the Graduate Faculty of

Swanson School of Engineering in partial fulfillment

of the requirements for the degree of

Master of Science

University of Pittsburgh

2017

UNIVERSITY OF PITTSBURGH

SWANSON SCHOOL OF ENGINEERING

This thesis was presented

by

Hsiang Ling Juan

It was defended on

April 7, 2017

and approved by

C. Isaac Garcia, PhD, Research Professor

Department of Mechanical Engineering and Materials Science

Qing-Ming Wang, PhD, Professor

Department of Mechanical Engineering and Materials Science

Susheng Tan, PhD, Research Assistant Professor

Department of Electrical and Computer Engineering

EFFECT OF TEMPERATURE RATIO (T_S/T_M) AND TIME ON THE SINTERING BEHAVIOR OF METALLIC 316L STAINLESS STEEL COUPONS COUPONS PRODUCED USING JET-BINDER TECHNOLOGY

Hsiang Ling Juan, M.S.

University of Pittsburgh, 2017

The present study investigates the microstructural, grain growth evolution and densification of metallic samples using water-atomized 316L stainless steel powder printed by Jet-Binder technology. To achieve a high final densification, the relationship between temperature ratio (T_S/T_M), where T_S is the sintering temperature and T_M is the melting temperature, time and densification behavior have been explored. The green density of metallic parts printed using Jet-Binder additive manufacturing is very low. Therefore, to have higher density and better mechanical properties, sintering heat treatments are needed. During this process, sintering takes place by the atomic transport whereby particle bond together below the melting temperature. The important variables of sintering include: the sintering temperature (T_S) and sintering time. In theory, the temperature ratio (T_S/T_M) will produce the highest densification value, i.e.

98%. In order to get the higher density, understanding and control of overall microstructure is needed. By microstructural control is meant the control of the grain growth behavior sintering density and distribution of pores. During the different sintering stages, different mechanism will be discussed in this work. The major challenge was the control of the variables in the sintering process and its influence on the grain growth behavior and pores morphology.

TABLE OF CONTENTS

ACKNOWLEDGEMENTS ixii
1.0 INTRODUCTION 1
2.0 LITERATURE REVIEW 3
2.1 POWDER PRODUCTION AND CHARACTERIZATION 3
2.1.1 Materials Specification 3
2.1.2 Water Atomization 4
2.1.3 Gas Atomization 7
2.1.4 Binder Saturation 9
2.2 SINTERING 10
2.2.1 Overview 10
2.2.2 Sintering Model and Densification 12
2.2.3 Sintering Atmosphere 20
2.2.4 Pores Migration Mechanism and Pores structure 31
3.0 HYPHOTHESIS 42
4.0 EXPERIMENTAL PROCEDURE 46
4.1 GREEN PARTS PREPARATION 46
4.1.1 Powder Characteristic 46
4.1.2 Printing 47
4.2 SINTERING PROCESS 51
4.3 DENSITY MEASUREMENT 56
4.4 MICROSTRUCTURE ANALYSIS 57
4.4.1 Optical Microstructure Analysis 57
4.4.2 Etching for OM Analysis 58
4.5 GRAIN SIZE MEASUREMENT 58
4.6 FRATAL DIMENSION ANALYSIS 59
5.0 RESULTS AND DISCUSSION 61
5.1 DENSIFICATION RESPONSE 61
5.2 EFFECT OF SINTERING TEMPERATURE 62
5.3 EFFECT OF SINTERING HOLDING TIME 71

5.4 EFFECT OF SINTERING ATMOSPHERE 83
6.0 CONCLUSIONS 86
7.0 FUTURE WORK 89
BIBLOGRAPHY 90

LIST OF TABLES

Table. 1. Chemical composition of standard 316L stainless steel.....52
Table. 2. Sintering temperature and time parameters design for standard 316L. 53
Table. 3 316L stainless steel different particle size densification. 62
Table. 4. The densification of stainless steel 15μm with different holding time on different sintering temperature. 72
Table. 5. Densification of sintering at 1300 ℃ for 90mins in different atmosphere with different particle size. 84

LIST OF FIGURES

Fig. 1. Schematic of a water-atomization system.[3].....5
Fig. 2. Scanning electron micrograph of a water-atomized 316L stainless steel powder.[4].....6
Fig. 3. Schematic of gas-atomization system.[3].....7
Fig. 4. Scanning electron micrograph of a gas-atomized 316L stainless steel powder.[4].....8
Fig. 5. Two-particle model for initial stage sintering (a) without shrinkage and (b) with shrinkage.[10].....13
Fig. 6. Material transport mechanism during sintering.[11].....13
Fig. 7. Development of the inter-particle bond during sintering.[9].....15
Fig. 8. Schematic of pore shrinkage during sintering: (a) just before the pore isolated, (b) shrinkage stage, (c) final stage[13]. 21
Fig. 9. Comparison of different atmospheres influencing the sintered density and grain size for a SS 422. 24
Fig. 10. Model of the pressure for different sintering atmospheres for a closed, shrinking pore. Arrows indicate pressure differences between pore and atmosphere. 25
Fig. 11. Data on the sintered density versus sintering temperature for a mullite LPS with a zirconia-alumina additive.[21].....26
Fig. 12. Final stage sintering data for ZnO doped with Sb_2O_3.[16].....27
Fig. 13. Densification rate vs. porosity for 95W alloy sintering at 1470℃.....30
Fig. 14. Density vs. sintering time for 95w alloy at 1460℃ for various assumed gas diffusivities through matrix.....30
Fig. 15. Conditions for pore stability: variation of dihedral angle for pore stability with the number of grains surrounding a pore.[28].....32
Fig. 16. Schematic of the pore structure change with sintering. [9].....33
Fig. 17. Two porous microstructures during sintering. (a) Densification is associated with pores located at edge. (b) No densification is associated with pores isolated in grains. [9].....33

Fig. 18. Possible mechanism of pore migration with a grain boundary.[10].....34
Fig. 19. Interaction of pore and grain boundary on grain size and pore size.[30].....37
Fig. 20. Schematic illustrating motion of pores attached to (A) disappearing grain, and (B) growth grain.[32].....40
Fig. 21. M-Flex powder bed binder jet 3D Printer.....48
Fig. 22. Binder jetting 3D printing process: (a) printing 2D pattern by using binder (b) binder drying (c) spreading a powder layer. 50
Fig. 23. Curing furnace. 51
Fig. 24. Powder box. 51
Fig. 25. Melting temperature of the standard 316L stainless steel by JMatPro. 52
Fig. 26. Sintering process steps example for 316L stainless steel sintering at 1356°C for 90 mins. 54
Fig. 27. Archimedes methods for holding the test specimen when weighing in water. 57
Fig. 28. Calculation of fractal dimensions with box-counting method.....60
Fig. 29. Densification (%) versus temperature (ºC).....63
Fig. 30. Optical micrographs of the 316L stainless steel (particle size 15μm) sintered at (a) 1300 ºC, (b) 1356 ºC, (c) 1366 ºC and (d)1380 ºC for 90 mins sintering in argon. 65
Fig. 31. Schematic of sintering behavior for 316L stainless steel with particle size 15μm showing the grain size versus densification and the schematic of pores migration. 67
Fig. 32. Sintering data for 316L stainless steel shows the grain size versus temperature. 69
Fig. 33. Grain size versus temperature of sintering 316L stainless steel 15μm for different holding time. 69
Fig. 34. Variations of density and pores fractal dimension with sintering temperature. 70
Fig. 35. Densification versus holding time at different sintering temperature for 316L stainless steel 15μm. 72
Fig. 36. Optical micrographs of the 316L stainless steel (particle size 15μm) sintered at 1356 ºC for (a) 90mins, (b) 360mins and (c) 24hrs. Sintered at 1300 ºC for (d) 90mins, (e) 360mins and (f) 24hrs in argon. 74
Fig. 37. Grain size versus holding time at the different sintering temperature for 316L stainless steel 15μm. 75

Fig. 38. Relationship between pores density and holding time at different temperatures. 76
Fig. 39. Variations of density and pores fractal dimension with holding time. 77
Fig. 40. 316L stainless steel 15μm grain growth data of microstructures fitted according to: (a) Coble's model of lattice diffusion-controlled pore drag and (b) Coble's model of surface diffusion-controlled pore drag. 79
Fig. 41. 316L stainless steel 15μm grain growth data of microstructure fitted according to: (a) Kang's model of lattice diffusion controlled densification and (b) Kang's model of grain boundary diffusion controlled densification. 82
Fig. 42. Comparison of vacuum and argon atmosphere influencing the densification with different particle size....84
Fig. 43. Optical micrographs of the 316L stainless steel sintering at 1300 ºC for 90 mins in different atmosphere (a-c) vacuum and (d-f) argon; with different particle size (a) 15μm, (b)24μm, (c)41μm, (d)15μm, (e)24μm and (f)41μm. 85

ACKNOWLEDGEMENTS

Firstly, I would like to thank to my advisor, Dr. C. I. Garcia, for his patient guidance and instructive suggestions through my experiments. I would never finish this thesis without his help and supports. I would also like to thanks to my committee members: Dr. Qing-Ming Wang and Dr. Susheng Tan, for their time and help to make this thesis better.

Secondly. I would like to thank to my group members, Zhou Yu, Rafael Landa, Louis B. Kish and Zhan Fang Wu, for their useful experience in my research and generous help of experimental devices.

Finally, I would like to thank to my parents for their generous support and encouragements!

Thanks to them all!

1.0 INTRODUCTION

Additive Manufacturing (AM) is a process that translate the 3D model data into physics real product in a fast and easy way. A set of 2D data of finite thickness put into the AM machine, these 2D data in the AM machine that can be output in a layer-by-layer to form physical parts.[1]

The printing methods can be divided into two groups. The first one is material jetting that is during the process part of the materials are distributed from a print bed. Examples of this kind of techniques are: Selective Laser Melting (SLM), Electron Beam Melting (EBM) and Laser Engineered Near Shaping (LENS). In these processes, a small product can be completed in a very short time and have a fine microstructure due to the directly rapid solidification. However, this system needs to be used under a protective atmosphere to avoid oxidation and heat transferring. The working area is relatively small, which might not be directly applicable to large industrial parts.[2]

Another 3D printer process is the binder jetting where the binder is printed on the powder bed in order to form the cross-section part.

Compared to Material Jetting, Binder Jetting has some distinct advantages. First, unlike other techniques need to apply heat source when using laser or welding to melt the powder, the Binder Jetting system will not have distortion by residual stress under heat. Second, the Binder Jetting system can print much larger components and is more cost-efficient. Third, Binder Jetting does not need a support structure, this implies shorter printing time and material cost-savings. However, the products fabricated by Binder Jetting have several shortcomings compared to Material Jetting: (a) poor density and surface finishes, and (b) substantial shrinkage during sintering. Sintering after printing is a common way to enhance the strength and densification.

In this study, the Power-binder Jetting system called M-flex was used to fabricate metallic components using stainless steel 316L water atomized powder. The important variables that have been investigated included: sintering temperature, heating holding time and furnace atmosphere. The present research focused on the relationship between temperature ratio(T_S/T_M) and the pore-boundary interaction mechanism during sintering.

2.0 LITERATURE REVIEW

2.1 POWDER PRODUCTION AND CHARACTERIZATION

2.1.1 Materials Specification

316L stainless steel powder is used since its good overall mechanical properties, especially good strength at evaluated temperature and superior corrosion resistance behavior, are suitable for a wide range of application. 316L type is an austenitic chromium-nickel stainless steel containing a small amount of molybdenum. Molybdenum is especially effective in increasing crevice and pitting forms of corrosion resistance.

The goal of stainless steel powder production is to control both chemical and physical properties, such as composition, particle size, particle size distribution and particle shape. Stainless steel powders used for injection molding are generally made by atomization technique. There are four types of atomization technique, made by gas, water, hybrid gas-water or centrifugal atomization. The two most widely used technique are water atomization and gas atomization, which always put together for comparison.

2.1.2 Water Atomization

In water atomization system, steels are melted in an induction furnace and allow liquid metal via a runner, flowing into a tundish. In the atomization tank, the melted steel stream is separated and rapidly quenched by high pressure water jet into steel powder. For low-oxygen-content powder, the tank is filled with water and purged with nitrogen to avoid air leakage. Fig. 1. show a schematic of a water-atomized system. To produce a “good” 316L stainless steel powders requires to control as low as possible oxygen contents and particle surfaces. The particle shape and oxidation are the two main differences usually investigated between water- and gas-atomization.

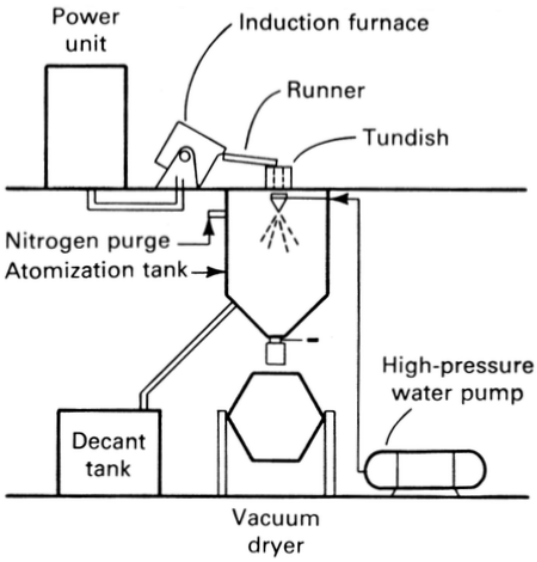

Fig. 1. Schematic of a water-atomization system.[3]

Since the heat capacity of water is larger than gas, the heat is extracted faster and the droplets solidify more rapidly in water atomization. Another way to say is the cooling rate in water atomization is higher than in gas atomization, which resulting in irregular shape and rough particle surface as show in Fig. 2.

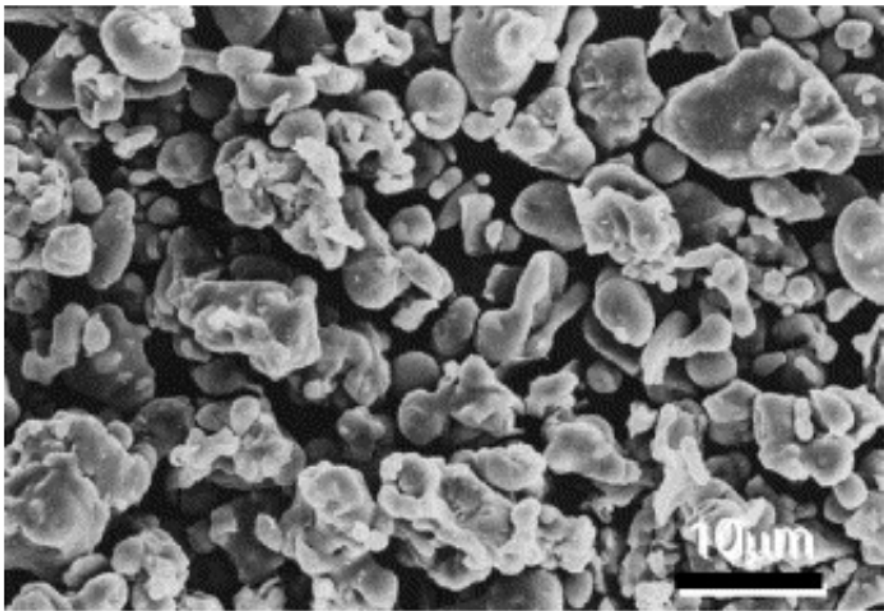

Fig. 2. Scanning electron micrograph of a water-atomized 316L stainless steel powder.[4]

Even though the atomization tank has been purged with an inert gas to minimize oxidation, the powder still partly becomes oxidized due to the reaction as below:

$$xM + H_2O \rightarrow M_xO_y + H_2 \qquad (1)$$

where M is metal element.[3]

The particles will have more irregular shape and the particle size distribution will be wider than gas-atomization. In fact, the surface condition of water-atomization can also occur by the formation of oxidation surface.

In gas-atomization, the major factors controlled the final particle size is flow rate and flow pressure. In water-atomization, particle size is controlled by water pressure; higher pressures produce finer powders and vice versa.

2.1.3 Gas Atomization

In gas-atomization system, steels are melted in a vacuum induction melter and pass through a nozzle. Liquid steel stream is fabricated into small particles by high pressure gas at the tip of the tundish, shorten the distance between liquid metal and gas to maximize the energy transfer from the gas to the liquid metal. It can produce a narrower particle size distribution. The Schematic process of gas-atomization system is shown in Fig. 3.

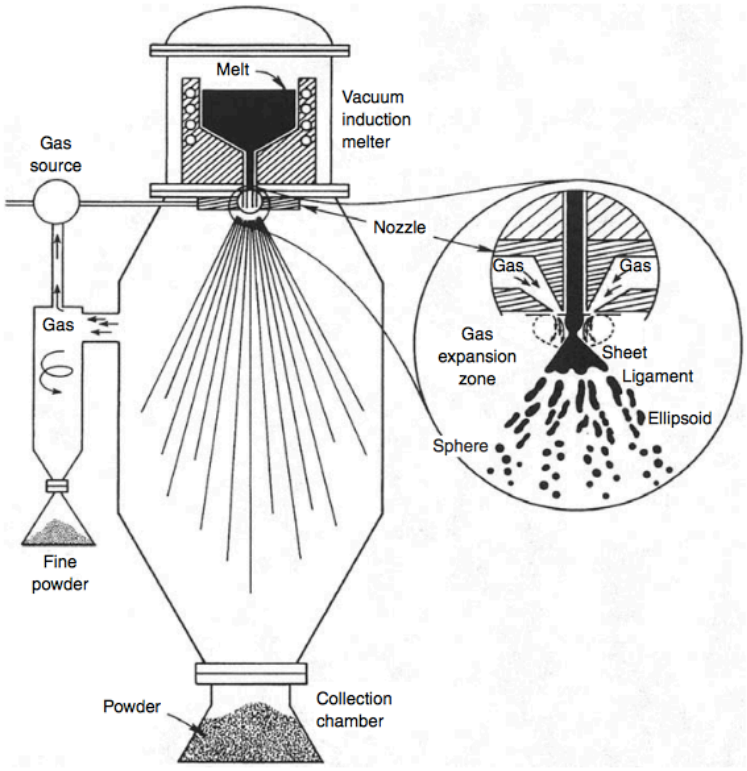

Fig. 3. Schematic of gas-atomization system.[3]

Typically, gas-atomized stainless steel powders are spherical and have high packing densities. Fig. 4. show a SEM of gas-atomized 316L stainless steel powder. Similar as water-atomization, in gas-atomization the final particle size depends on metal flow rate, gas flow rate (or gas pressure), gas type, nozzle dimensions and liquid metal temperature. Smaller particle size requires high gas pressure which need high gas energy and large amount of gas consuming.[5]

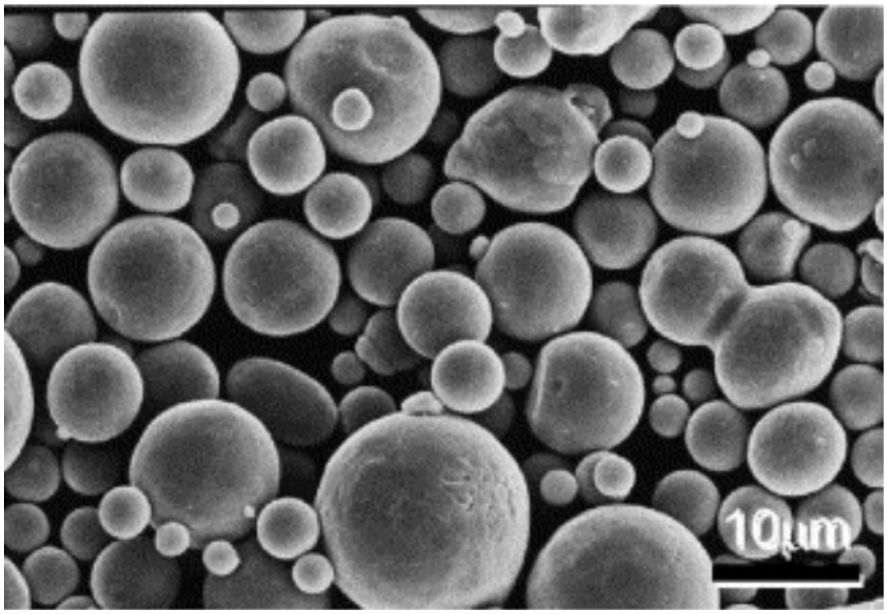

Fig. 4. Scanning electron micrograph of a gas-atomized 316L stainless steel powder.[4]

However, water-atomized powder is more economical and has faster thermal kinetics due to the irregular shape particle, enable to get the high density and high strength at lower temperature compare to gas-atomized powder.[6]

2.1.4 Binder Saturation

Binder is a temporary glue for connecting powder into the desired shape and holding the particle in that shape until the beginning of sintering. Although binder should not affect the final composition due to it will be removed during sintering process, it is still important at the beginning of shaping. The saturation of binder will influence the printing quality which contributed the green density. The definition of binder saturation level is the percentage of volume occupied by binder in each layer, usually at range of 35-100%.

A recent study focus on dimensional accuracy and surface finish in binder-jetting AM of 420 stainless steel. It was identified that binder saturation and layer thickness affect surface finish and initial green density; drying time had most influence on the shrinkage.[7] Another optimization study focused on print parameters effect on mechanical strength in binder-jetting AM of 316L stainless steel. It was found that saturation level 70% and feed-to-powder ratio at 3 has the best mechanical strength.[8]

2.2 SINTERING

The effects of three sintering factors: sintering temperature, sintering time and sintering atmosphere, on the final density were investigated. The optimum sintering condition was proposed and conducted in the experiments.

2.2.1 Overview

Sintering is a thermal treatment for bonding particles into a solid structure through mass transport or diffusion process that occur on the atomic scale. The bonding leads to improved strength and a reduced system energy.[9] In general, to produce the sintering part with reproducible properties need to design its microstructure by controlled sintering variables. Microstructural control means the control of sintered density, grain size and distribution of pores. The final goal of microstructure control is to become a fully dense body.

The variables of sintering process can be divided into two: material variables and process variables.[10] The variables related to the raw materials (material variables)

include chemical component of powder, powder size, powder shape etc. These variables influences the grain growth and densification. The material variables are already discussed in section **2.1**. Another type of variables is related to the thermodynamics (process variables), such as sintering temperature, heating and cooling rate, holding time, pressure, atmosphere etc. This study is more focused on the effect of the temperature and atmosphere on sintering ability of powder. To investigate more about process variables, we need to know the sintering process first. Sintering process can be divided into three stages: initial, intermediate and final.

2.2.2 Sintering Model and Densification

Initial Stage

Neck growth between contacting particles is an obvious aspect of initial sintering. The initial stage is defined neck size ratio (X/a) < 0.3. Where X is the radius of neck and a is the radius of particle. [9] During this stage the kinetics are dominated by the curvature gradients located near the inter-particle neck. Due to powder particles have complex shape and different size, it is hard to explain in a simple way. However, a simplified two-sphere geometry particle model is used to explain neck growth in the initial stage sintering. Fig. 5. shows geometrical model for two particles: left one (a) without shrinkage and right one (b) with shrinkage.[10]

In Fig. 5. (a), the distance between particles does not change but the neck size increases with the increase of sintering time. In Fig. 5. (b), the neck size is increased with the sintering time increased and the bulk transport between the particles results in the shrinkage result.

During the neck formation, to determine the mass flow in response to the driving force for the sintering mechanisms in the two-particle model is show in the Fig. 6.[11]

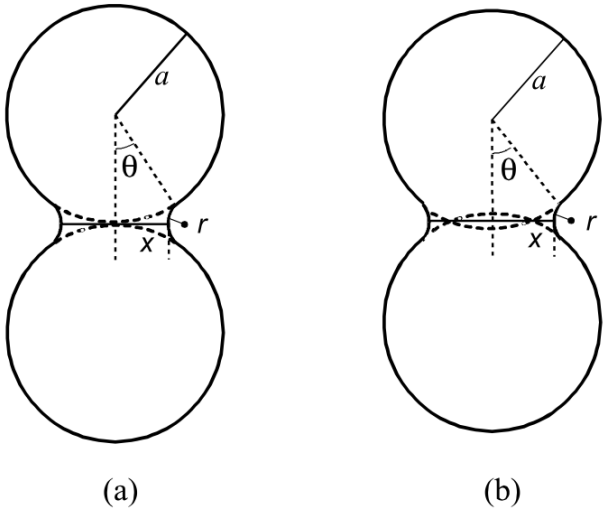

Fig. 5. Two-particle model for initial stage sintering (a) without shrinkage and (b) with shrinkage.[10]

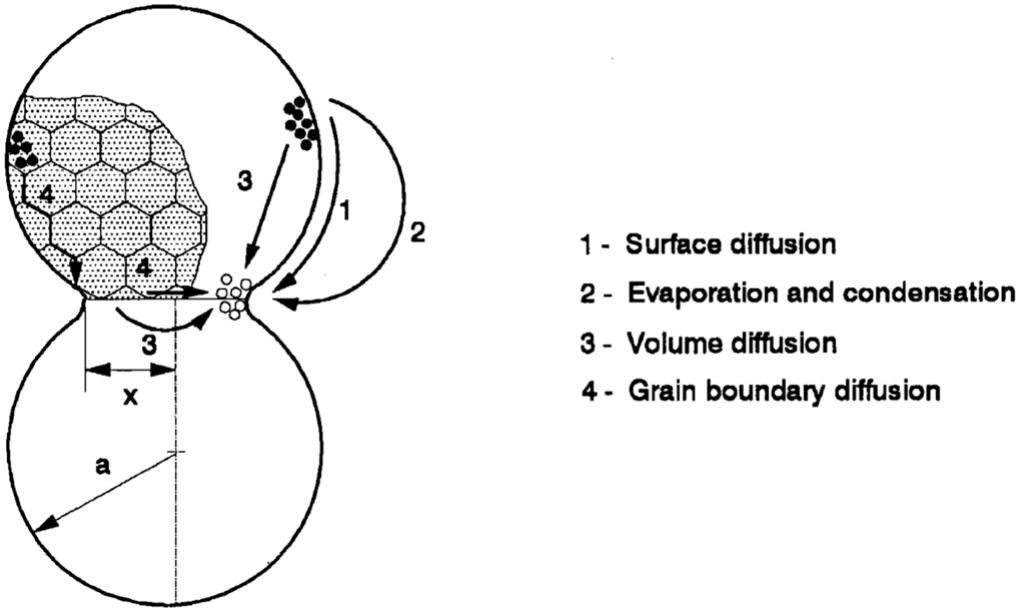

Fig. 6. Material transport mechanism during sintering.[11]

There are several mass paths in sintering, and two main mechanisms are surface transport and bulk transport. Evaporation-condensation and surface diffusion are the common surface transport. A weight loss by reacting with the sintering atmosphere is

an indication of evaporation-condensation. In most of materials the evaporation-condensation contributions are small and can be ignored. Surface diffusion also produce a loss of surface area during sintering but no shrinkage.

For bulk transport process, there are two main mechanisms: volume diffusion and grain boundary diffusion. Volume diffusion is active in most sintering systems, but the lower activation energy for grain boundary diffusion makes this dominant in many cases. Grain boundary diffusion is very important to the sintering densification of most metals. The inter-particle boundary provides a path. Generally, bulk transport processes are active at higher temperature.

While both surface transport and bulk transport promote the neck growth, the main difference is in shrinkage during sintering. The surface transport produce neck growth without shrinkage due to the mass flow only at particle surface, Fig. 5. (a) shows the surface transport mechanism as applied to the two-particles model without shrinkage. However, the bulk transport produce neck growth from the internal mass sources, Fig. 5. (b) shows the bulk transport mechanism as applied to the two-particles model with shrinkage. However, the initial stage sintering model for shrinkage is only valid for the first 3% of shrinkage.

The densification rate increased with decreased particle size. Because of the surface diffusion and grain boundary diffusion are enhanced by a decreasing particle size. On the other hand, coarse powders require higher sintering temperature or longer sintering time.

Intermediate Stage

The intermediate stage is most important in the sintering stages for densification and the sintered properties. The driving force is elimination because the curvature has largely been smoothed than the initial stage and surface energy decreased. During this stage the neck growth and X/a ratio increase. When neck formed between two particles, pore channel formed at the three grains edge show in the Fig. 7. Along the process of sintering, the pore channel will break and form the isolated pores. In fact, the pore size distribution and pore shape distribution are controlled during this stage.

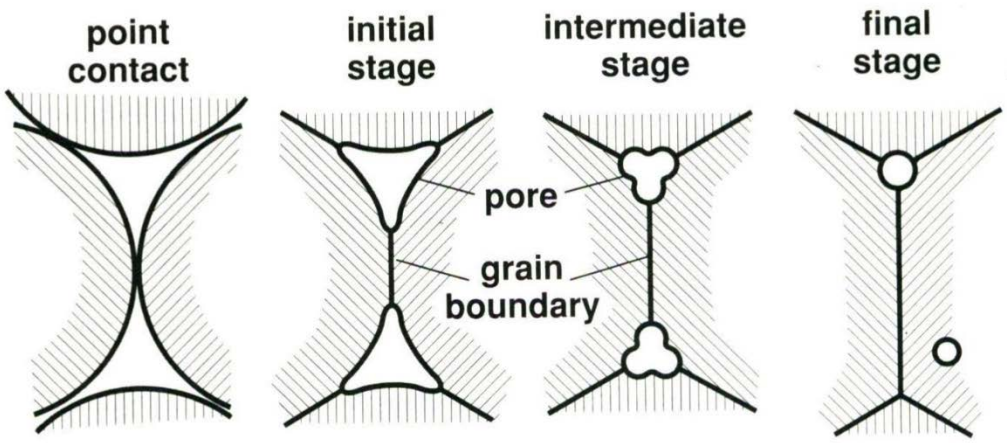

Fig. 7. Development of the inter-particle bond during sintering.[9]

In order to get the high density, it is necessary to limit grain growth during sintering. The rate of grain growth depends on the mobility of the grain boundary. First, assume no pore-boundary separate, the grain size versus time gives a relationship as follows:[12]

$$G^C = {G_0}^C + Kt \ \ exp\left[\frac{-Q_g}{kT}\right] \quad (2)$$

$$\varepsilon = 4\pi\left(\frac{r}{G}\right)^2 \quad (3)$$

where G is the grain size, K is the material constant, t is the time, Q_g is the effective model for pore-grain boundary, r is the pore radius and ε is the porosity.

Eq. (2) shows the relationship of grain size usually increased with time. Assuming pore is attached on the grain boundary, this relation shows grain size will increase when the pores coalesce or porosity is decreased.

Second, the densification rate during intermediate stage depends on diffusion of vacancies away from the pore. The rate of pore elimination can be expressed shows as follows:

$$\frac{\mathrm{d}\epsilon}{\mathrm{dt}} = -JAN\Omega \quad (4)$$

$$\frac{\mathrm{d}\epsilon}{\mathrm{dt}} = -\frac{96\pi\gamma\Omega D_0 exp\left[-\frac{Q}{kT}\right]}{kTG^3} \quad (5)$$

where ϵ is the porosity, J is the diffusive flux, A is the area over which diffusion act,

N is the number of pores per unit volume and Ω is the atomic volume.

Combined with Fick's First law $J = -D\nabla\Phi$

$$\frac{\mathrm{d}\rho}{\mathrm{d}t} = \frac{-\mathrm{d}\epsilon}{\mathrm{d}t} \quad (6)$$

$$\rho + \epsilon = 1 \quad (7)$$

$$\rho = \rho_i + B_i \ln\left(\frac{t}{t_i}\right) \quad (8)$$

$$\epsilon^{3/2} = C_i + {B_b}\Big/{t^{1/3}} \quad (9)$$

where ρ_i and t_i represents the density and the time at the beginning of the intermediate stage, C_i represents the conditions at the beginning of the intermediate stage and B_b contains several geometric and material properties including the diffusivity, surface energy, atomic volume and grain boundary width.

Eq. (2) & Eq. (3) show clearly the rate of densification is dependent on the grain size, density, temperature and time; however, the temperature effect is dominant among them.

Particle size has a huge effect on pore size. The initial finer particle cause the small pore size, then the small pore will shrink by grain boundary diffusion and surface diffusion. As the pores shrink considerably, grain growth can be enhanced.

The neck growth continues in the intermediate stage; however, the neck shape is lost and the pores become smooth and have an interconnected, cylindrical structure.

The driving force is the interfacial energy, including both the surface and grain boundary energy. At this point, the cylindrical pores collapse into spherical pores which are not effective in slowing grain growth and do not contribute to the densification. Consider the rate of diffusion, grain growth and pore motion are all related to temperature, it is the key of microstructure changing.

As the temperature increased, the rate of the grain boundary motion increased. Grain boundary diffusion is dominated at higher temperature and allows faster densification versus pore coarsening.[12] Densification in this stage is dominated by grain boundary diffusion and volume diffusion. If the pore motion slower than the grain boundary motion, then the pore will break away from grain boundary and be isolated in the grain. Separation of the pores from the boundaries limits the final density possible for sintering. Furthermore, the formation of the pores or the second phase is expected to control the grain growth.

The intermediate stage is relied on connection of pores and grain boundaries to maintain densification. It is important to minimize separation between pore-grain boundary by temperature control or reduced the initial particle size distribution. This implies that a successful sintering treatment should be done in the temperature range where grain growth is inhibited or there is no significant grain boundary mobility.

Final Stage

In this stage, the kinetic is very slow and pores which isolated in grains are shrink by volume diffusion mechanism. The driving force is strictly the elimination of the pore-solid interfacial area.

Grain growth forces the grain boundary to be curved, and increase the grain boundary area, thus it will contact with a slow-moving pore. A pore and a grain boundary have a binding energy, when the pore is contact with the grain boundary then total area reduced and binding energy decreased. Additionally, the binding energy increases with the increases of porosity and pore size, and decreases during densification.

The dominant mechanism change from grain boundary diffusion to volume diffusion at the final sintering stage is due to the increase in pore size that results from

pore coalescence with grain growth. Pores shrink if the rate of volume diffusion is high and the rate of coalescence is low. Alternatively, the pore coalesced at a low diffusion rate and high grain growth. It is because the increase in pore size that result from pore coalescence with grain growth. With extended heating time, pore coarsening will cause the pore size increase while the pore number decrease.

After intermediate sintering stage, the pores are rounded and expected breakaway from grain boundaries while isolated in the grains. When the pores are isolated in the grain, the final densification is strongly affected by the sintering atmosphere since the gas is trapped in the pores. A homogenous grain size and a soluble gas provide densification in the final stage. More details about sintering atmosphere will be illustrated at next section.

2.2.3 Sintering Atmosphere

The effect of entrapped gas in pore can be calculated for various experimental data, as shown by Yoon and Kang.[13] They calculated the final density and densification kinetics. When the pressure of entrapped inert gas equal to the capillary pressure of the

pore, the pore stop shrinking and reach the maximum density. Fig. 8. shows the driving pressure change during the pore shrinking.[14]

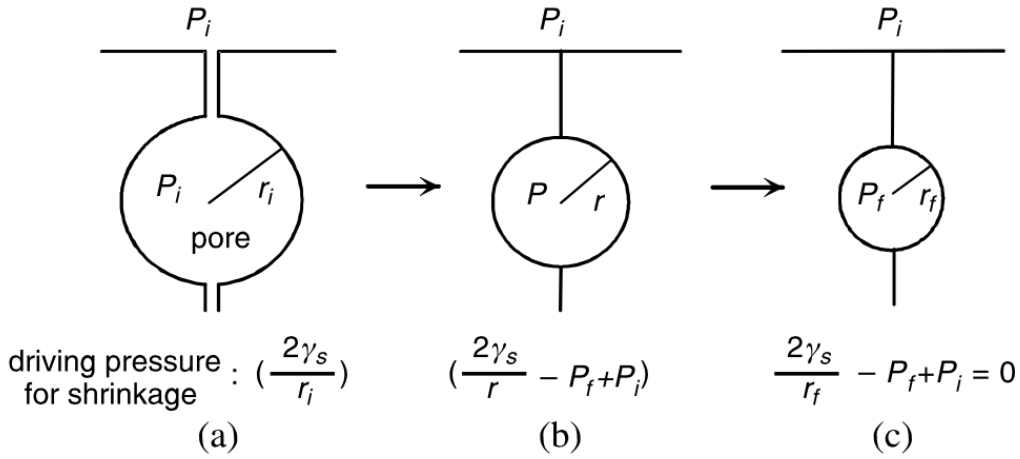

Fig. 8. Schematic of pore shrinkage during sintering: (a) just before the pore isolated, (b) shrinkage stage, (c) final stage[13].

At approximately 92-94% density, the pores make a rapid shift to a closed structure. If there is a trapped gas in the closed pore, then the densification rate is controlled by the internal gas pressure. The gas pressure in an isolated pore is different to that outside the compact, pore is either extend by an excess internal pressure or shrink by an excess external pressure.[10]

When sintering in vacuum the compact densifies and all pores can be eliminated, but in atmosphere-based sintering the pores grow and become stable while grain growth continues with little resistance. Pressure in the pore decrease as it enlarges, allowing faster pore growth with swelling.[15]

Initial pressure and initial pore size are also important factors for the densification. As the initial gas pressure is high or initial pore size is larger, higher density is not possible while gas is trapped in the pores.[16] The presence of a gas in the pore will also limit the amount of final stage densification. Alternatively, if the initial pore radius is very small (less than a few microns) the pore still shrink and have essentially no effect by the entrapped gas.

The sintering atmosphere influences sintered bonding and densification. Accordingly, in real process, it is more complicated and a key to ensuring the properties. There are several types of atmospheres: air, inert gas, hydrogen, dissociated ammonia, nitrogen-based and even vacuum.[9] The initial atmosphere is provided heat transfer and remove the polymer decomposition products from binder.

When the gas was trapped inside the pore, prolonged holding time at the sintering temperature causes a drop in the sintered densities and properties.[17] When the gas

pressure within the pores increase to balance the surface energy effect, no further densification will occur. This condition will happen when the entrapped gas is no solubility. Gas is trapped in the pores then gas solubility in the sintering material determines what happens.[18]

For example, the inert gas like argon or a gas which has a low solubility in the matrix like water vapor, is trapped within the pores, then it will hinder densification. Indeed, swelling is often seen during prolonged sintering due to pore coalescence. However, if the entrapped gas has some solubility and diffusivity in the matrix, like hydrogen, then it will gradually diffuse out as the pores shrink. Trapped hydrogen may decrease the densification rate, but will not prevent complete densification.[19]

There is an example by using varied atmospheres during sintering. C. Toennes and R.M. German sintering stainless steel in three different gas atmospheres: argon, vacuum and a cycle in which vacuum was backfilled with argon after hold for 60 mins at the sintering temperature.[20] Fig. 9. shows in the initial 60 mins of sintering the density curves are the same in three atmospheres; however, sintering in argon has lower density as compare to in vacuum for sintering times longer than 60 mins. It does not seem like due to a cleaning effect of the vacuum compared to the argon system because the initial

density is the same. It is more like that sintering in argon has a densification limiting effect when the pore becomes closed and filled-in gas. Argon does not dissolve in steel, when it trapped into pores the increasing pressure limited the densification. Fig. 10. gives model for the pressure condition of the different sintering atmospheres for a closed pore.[20]

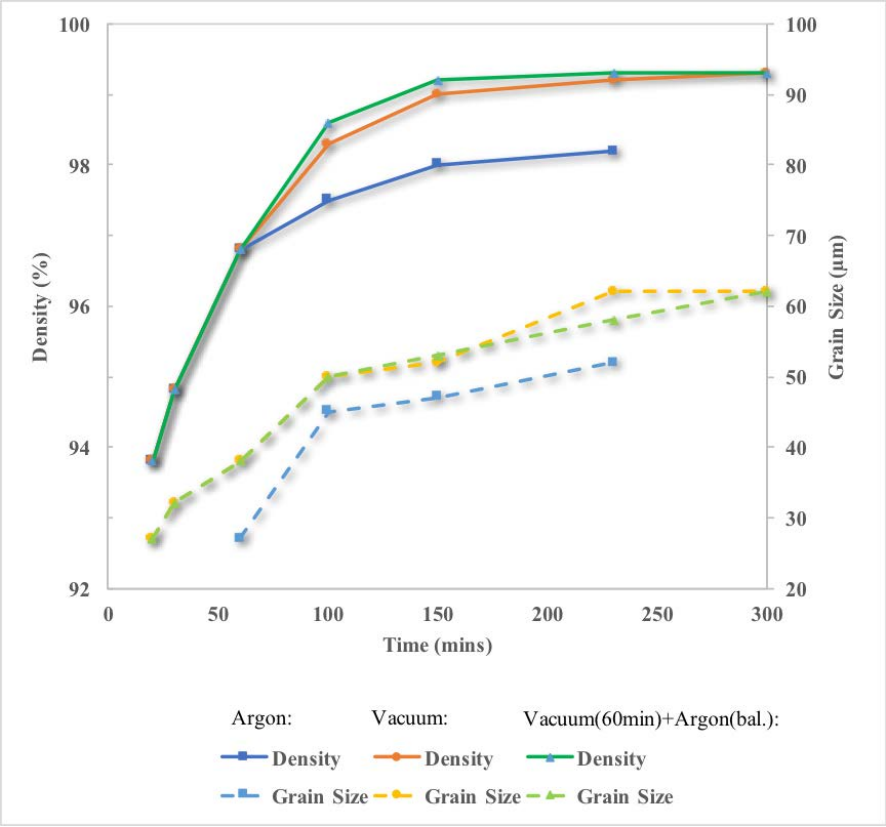

Fig. 9. Comparison of different atmospheres influencing the sintered density and grain size for a SS 422.

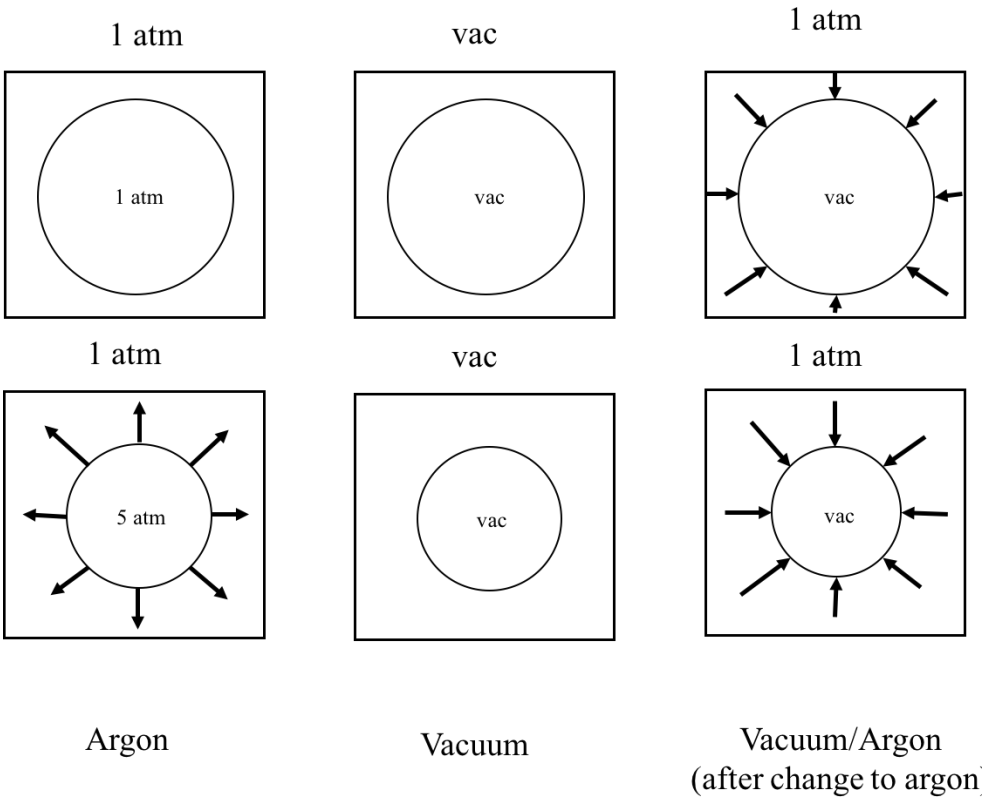

Fig. 10. Model of the pressure for different sintering atmospheres for a closed, shrinking pore. Arrows indicate pressure differences between pore and atmosphere.

Fig. 11. shows another example of retarded densification where high temperature reaction produces an insoluble gas.[17][18] The data reaches the highest sintered density at about 1300° C when the open pores disappeared, but decreased at higher temperatures. It is due to the expansion of closed pores which have gas trapped in it.

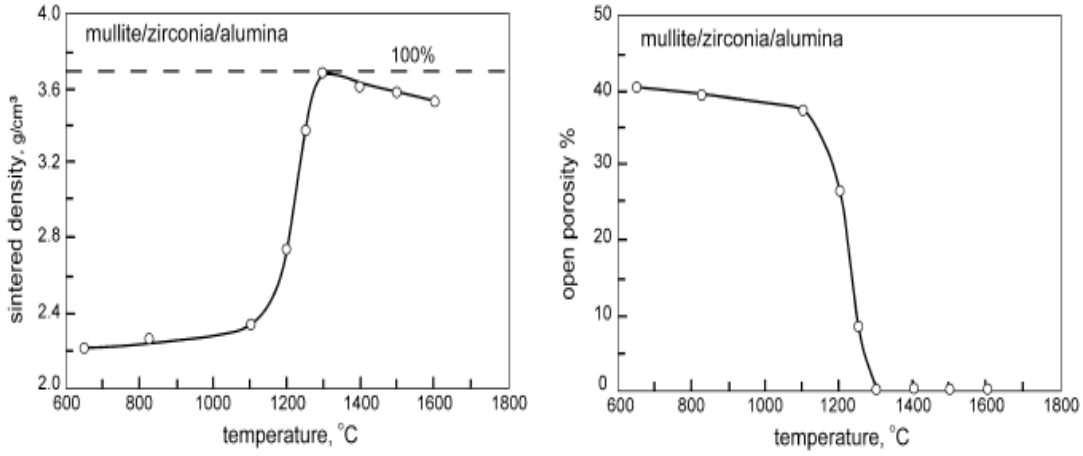

Fig. 11. Data on the sintered density versus sintering temperature for a mullite LPS with a zirconia-alumina additive.[21]

Fig. 12. shows a final stage sintered density decreased during the prolonged sintering time for three temperatures. Indeed, the highest density is come from the lowest temperature, where evaporation is low and pore coarsening is slow. Because pore coarsening leads to a reduced gas pressure in the pores, and cause the porosity increase.[16][15]

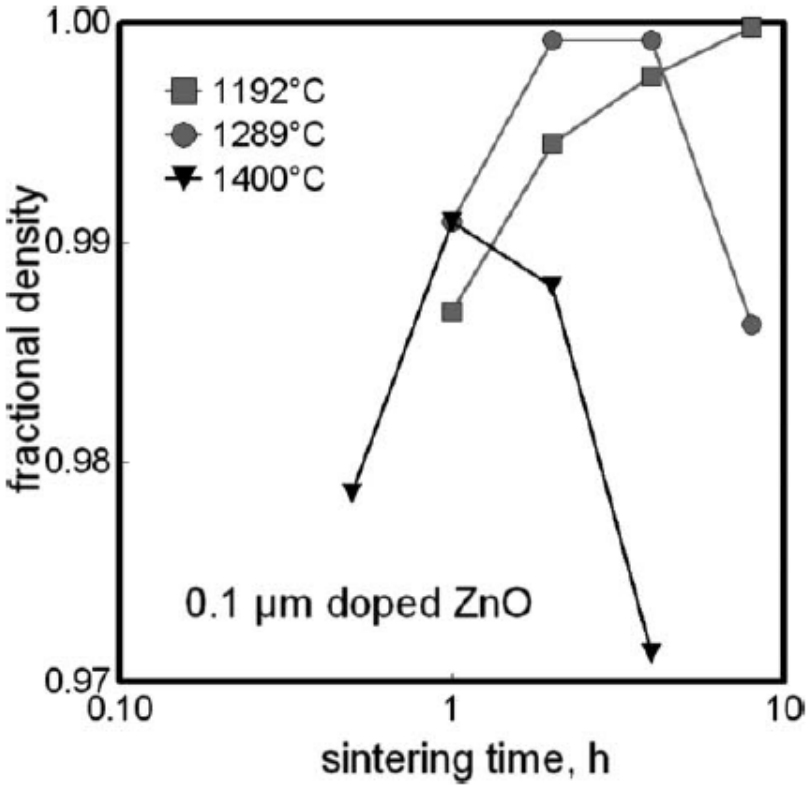

Fig. 12. Final stage sintering data for ZnO doped with Sb_2O_3.[16]

If the pore has a trapped gas, then it will influence the elimination rate of pore number. Pore coarsening works against densification, especially in cases where a gas exists in the pores.[17][22][23] In some cases, pore growth due to coalescence of the smaller pores, but also due to vapor production during sintering. In the extreme case, enormous pores as the gas accumulates inside the component to form a single large pore.

The effect of the sintering atmosphere is analyzed for final elimination. The elimination of the remaining pores is described by the final stage model of Markworth [24] as follows:

$$\frac{d\rho}{dt} = \frac{12\Omega D}{kTG^2}\left[\frac{2\Upsilon}{r} - P_g\right] \quad (10)$$

where r is the radius of pores, ρ is the fractional density, t is the time, dρ/dt is the densification rate, Ω is the atomic volume, D is the diffusivity, k is the Boltzmann constant, T is the absolute temperature, G is the grain size, Υ is the mean surface energy and P_g is the gas pressure.

During final stage densification, several processes interact to affect the observed sintering rate. By assuming spherical pores, the fractional porosity ε can be related to the pore radius r and the pore density N (number per unit volume).

$$\varepsilon = N\frac{4}{3}\pi r^3 \quad (11)$$

Additionally, the pore density and grain size G are related as follows:

$$G^3 = {}^{C}/_{N} \quad (12)$$

where C is the number of pores per unit grain volume.

However, if there is gas trapped in the pores, then densification influenced by the gas pressure in the pore. In the situation of entrapped gas is insoluble (such as argon gas), will be pressurized by pore collapse. Assuming ideal gas behavior:

$$P_g\varepsilon = P_c\varepsilon_c \qquad (13)$$

where ε_c is the porosity at the pore closure ($\varepsilon_c = 0.08$ in this analysis), P_c is the gas pressure at pore closure (usually ≈ 1atm). A combination of Eq. (10)-(13) gives:

$$\frac{d\rho}{dt} = \frac{12\Omega D N^{2/3}}{kTC^{2/3}}\left[\frac{2\Upsilon}{\varepsilon^{1/3}}\left(\frac{4\pi N}{3}\right)^{1/3} - \frac{P_c\varepsilon_c}{\varepsilon}\right] \qquad (14)$$

This equation predicts that densification will stop when the surface effect is balanced by the pore gas compression. Fig. 13. and Fig. 14. show the calculation of densification rate vs. porosity and density vs. sintering time by Eq. (10), (13) and (14).

In Fig. 13. Its shown the result of a reduction in the densification rate when the porosity decreased in insoluble atmosphere. In Fig. 14. is presented the elimination of the densification at the last stage is highly dependent on the gas diffusivity. Additionally, long sintering time allow coarsening by both diffusion and coalescence. Pore coalescence is thought to be the result of rapid grain growth.[18]

The increase of porosity with sintering time can be attributed to tiny pores containing certain gas can coalesce through the matrix. When the pores thus grow, the pressure exerted on the pore by the surface tension of the matrix will be decreased because of increased pore radius. Therefore, the total pore volume can increase.[25][26]

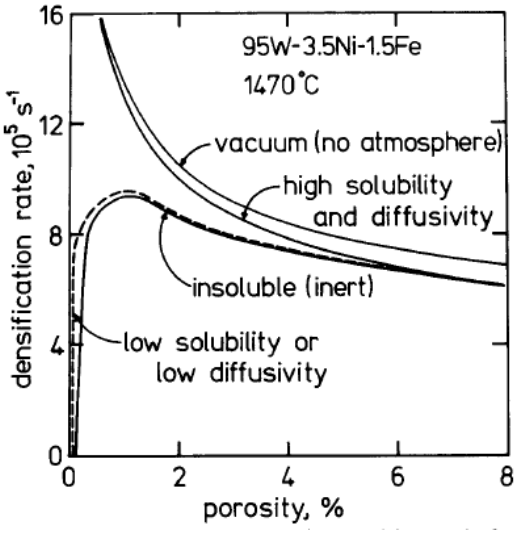

Fig. 13. Densification rate vs. porosity for 95W alloy sintering at 1470°C.

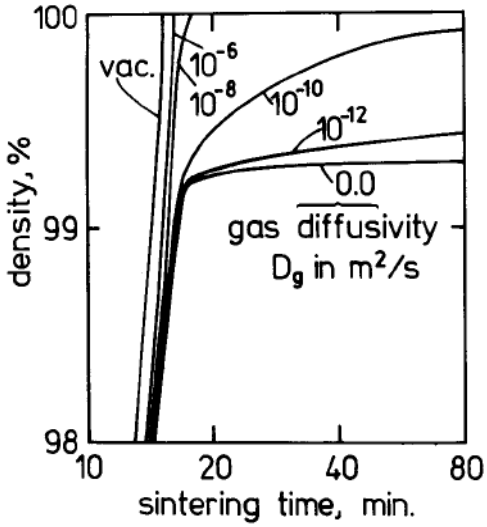

Fig. 14. Density vs. sintering time for 95W alloy at 1460°C for various assumed gas diffusivities through the matrix.

Pore coarsening leads to a reduced gas pressure in the pores and compact swelling. Therefore, pore pressure decreases as the pore coarsens, giving a net porosity increase.[16]

2.2.4 Pores Migration Mechanism and Pores structure

The pore can be thought as having a binding energy in relation to the grain boundary. This binding energy increase as porosity increase. Grain boundary as an atom source need a critical driving force for movement. For rough boundaries with random orientations, the critical driving force must be low. On the other hand, for the smooth boundaries with energy peak, the critical driving force must be higher than rough boundaries.[10]

In reality, grain boundary is not an ideal source with no energy barrier but a source need to concern varies with the nature of boundary, the angle between grains and the impurity near boundary. Fig. 15. shows the relationship between pore stability, dihedral angle and number of surrounding grains in the three-dimensional structure.[28] As the dihedral angle increases, the condition of pore and grain relation is increases. In general, the pores smaller than the average grain will stratify the shrinkage condition.

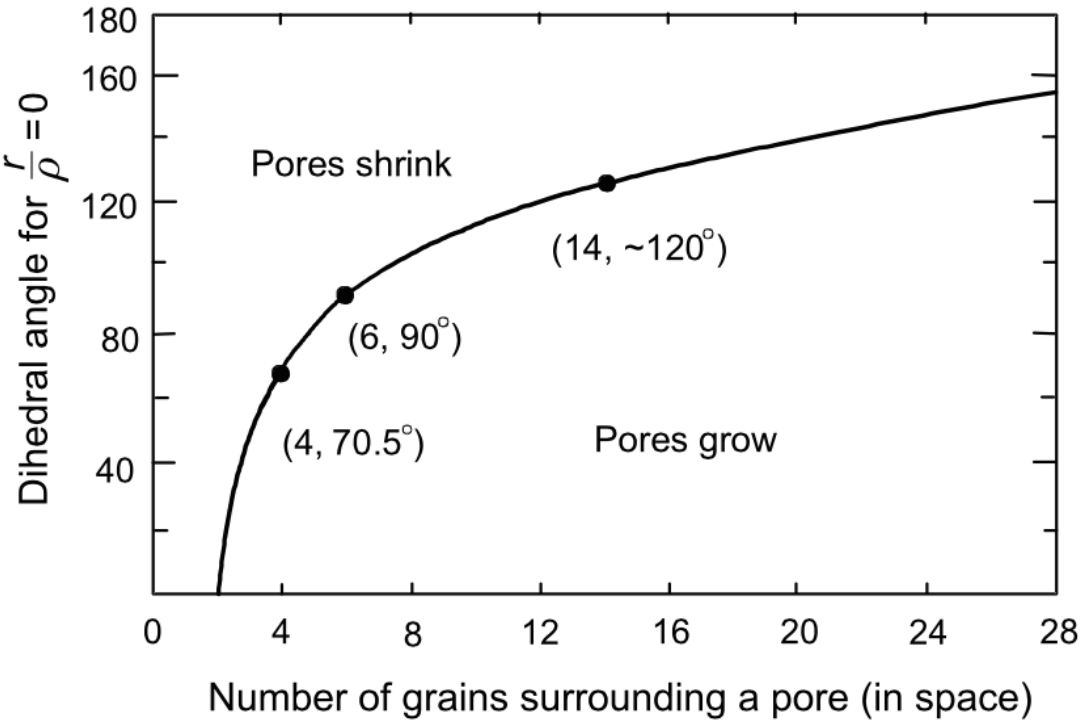

Fig. 15. Conditions for pore stability: variation of dihedral angle for pore stability with the number of grains surrounding a pore.[28]

Fig. 16. shows the microstructure transformation during the sintering. Initially, particles contact each other grow into necks. At this stage, pore structure is open and fully interconnected, although the pore shape is not very smooth. Grain boundaries emerge and the pores occupied the grain edge in an irregular shape, the system energy is lower because the pore reduces the total grain boundary area. After the initial stage, the grain boundary and pore configuration controls the sintering rate. At the beginning of the intermediate stage, the pore geometry is highly convoluted and the pores are located at grain boundary intersections.

Along the process of sintering, the pore channel will break and form the isolated pores. With continued sintering the pore geometry approaches a spherical shape where densification occurs by decreasing the pore radius. As the final stage of sintering begins, the pore structure collapses from an open, continuous network into discrete spherical pores. Consider the two extreme pore-boundary conditions, as show in Fig. 17.

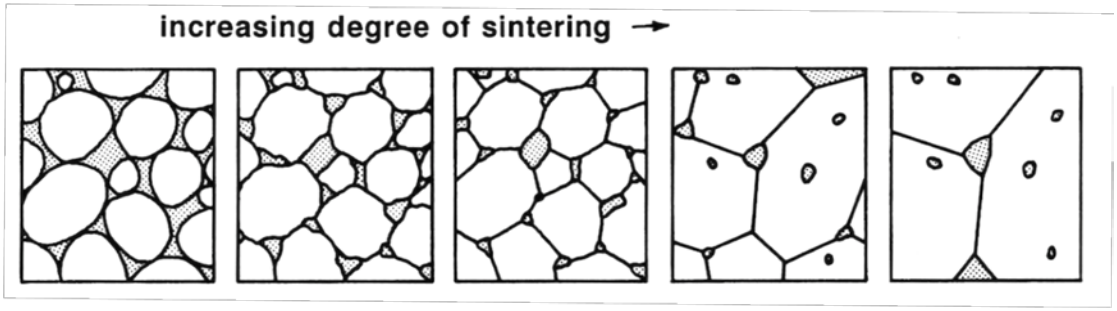

Fig. 16. Schematic of the pore structure change with sintering. [9]

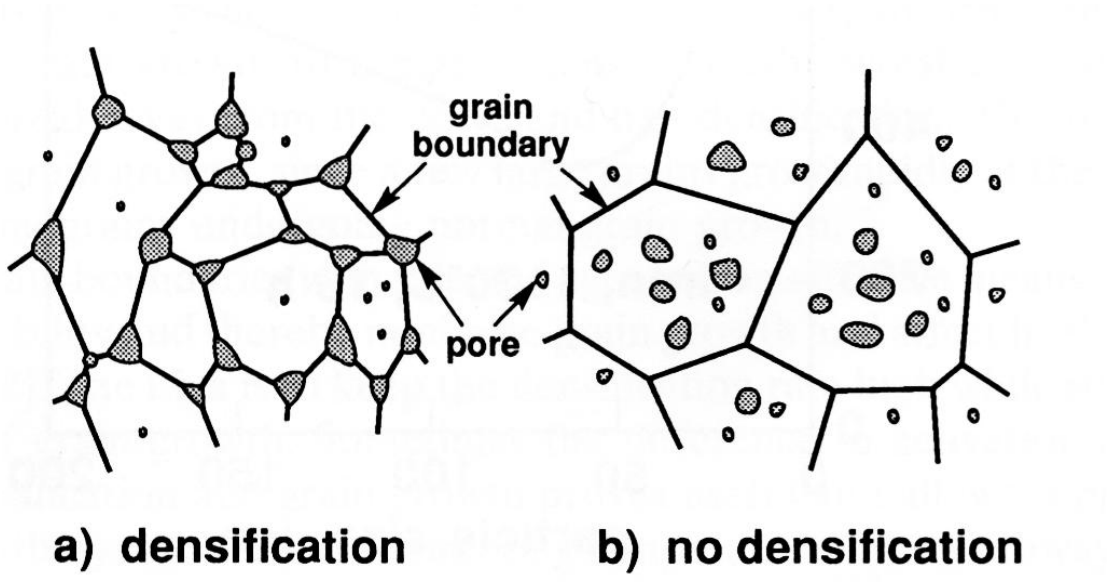

Fig. 17. Two porous microstructures during sintering. (a) Densification is associated with pores located at edge. (b) No densification is associated with pores isolated in grains. [9]

At the final stage of sintering, pores are present mostly at grain boundary and triple junction. Pores move together with grain boundary as the grain growth. If the pore is attached to the grain boundary and both move together, the pore velocity v_p is expressed as

$$v_p = M_p F_p \qquad (15)$$

where M_p is the pore mobility and F_p is the maximum inhibiting force of a pore against grain boundary.[29]

Fig. 18. shows a schematic of pores migration mechanisms include surface diffusion, lattice diffusion, gas diffusion and evaporation/condensation.[10]

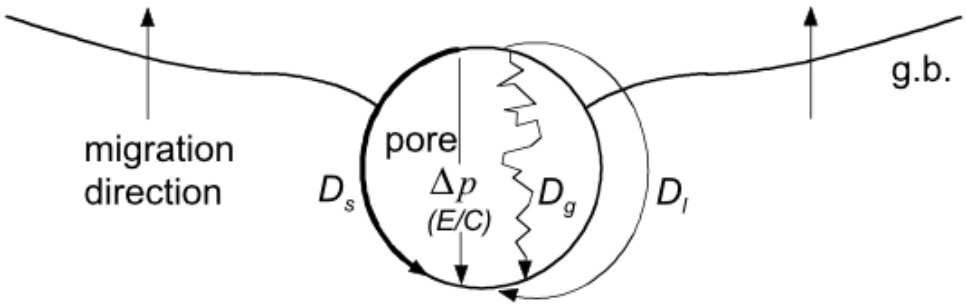

Fig. 18. Possible mechanism of pore migration with a grain boundary.[10]

When pores are present at grain boundary, the net driving force of grain boundary migration is the difference between the driving force for the boundary without pores and the restrain force of pores against boundary migration. The boundary velocity v_b is expressed as

$$v_b = M_b(F_b - NF_p) \quad (16)$$

where M_b is the boundary mobility and N is the number of pores per unit grain boundary area. Combined with the Eq. (15),

$$v_b = v_p = M_p F_p = M_b(F_b - NF_p) \quad (17)$$

and hence

$$v_b = \frac{M_b}{1 + N\left(M_b / M_p\right)} F_b \quad (18)$$

When pores are separated from the grain boundary, the pores are entrapped within grains and cannot be eliminated by sintering. Therefore, separation of pore and grain boundary is the limit of densification in sintering.

From Eq. (18) two cases can be considered;[30]

(i) $NM_b > M_p$,

(ii) $NM_b < M_p$ and

(iii)$NM_b = M_p$.

In case (i), system has a large number of large pores with low motilities at the beginning of the final stage sintering. Thus, pore migration controlled the grain boundary migration. However, as sintering proceeds, the separation can occur. If the pore isolated in grain, pore motion under the tension of a moving grain boundary is possible by volume or surface diffusion or even evaporation-condensation across the pore. It will be hard for the pore closed.

On the other hand, case (ii) applied a small number of small pores with high mobility pores and low grain boundary migration velocity. The pores do not affect the boundary migration during this condition. When grain growth and boundary migration are very slow, the separated pores will reattach with the boundary.

In case (iii), when M_b is equal to M_p/N in Eq. (18), the grain boundary mobility is the same as the pore mobility. The equal mobility condition on a grain size versus pore size can be calculated for many mechanisms of pore migration.[29][30] Fig. 19. shows the type of pore and boundary interaction on pore size and grain size.[30]

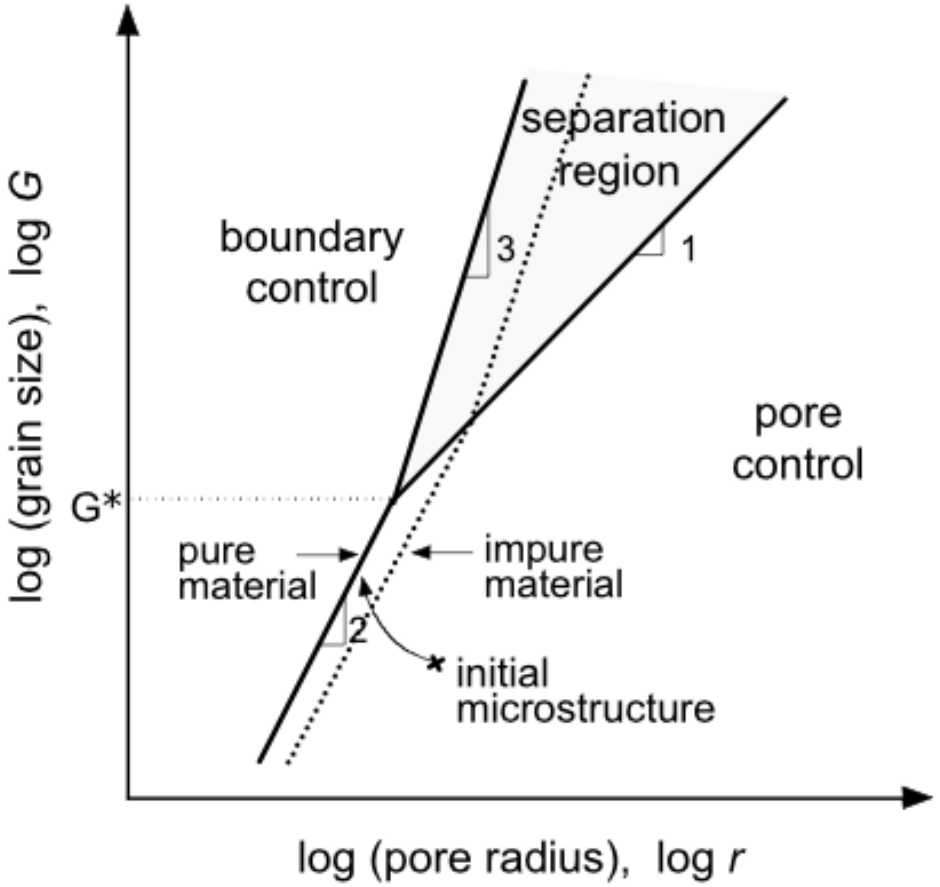

Fig. 19. Interaction of pore and grain boundary on grain size and pore size.[30]

The minimum grain size G^* is expressed as:[10]

$$G^* = \sqrt{\frac{\beta^4 \pi^3 D_s \delta_s \Omega}{16D\frac{1}{b}a^2}} \qquad (19)$$

where β is a constant which is determined by the real curvature of the boundary, δ_s is the thickness of surface through which diffusion occurs, Ω is the atom volume and a^2 is the atom area. It appears that grain growth improved or G^* increased could prevent the separation of pore and grain boundary.

The interactions between pore and grain boundary plays an important role in this stage. During sintering, the applied thermal energy affect pore migration and grain boundary migration. There are two possibilities for the interaction between pore and grain boundary: One is the pores are dragged along with the moving grain boundary during grain growth. Another is the grain boundaries break away from the pores and leaving them isolated in the interior grain.

If the pores remain attached to the grain boundaries, then they can shrink. If pores are separated from grain boundaries will remain stable and resist densification. Accordingly, grain growth is detrimental to sintering since the grain boundaries become more widely spaced, have less proximity to pores, and often move faster than the pores. Indeed, rapid grain coarsening generates conditions where sintering prematurely terminates with considerable residual porosity.

The way to get the high densification is preventing the separation between pore and grain boundary and gradually increasing in grain growth. If the pore and boundary become separated, the system energy will increase in proportion to the amount of newly created interfacial area. A lower grain boundary mobility decreases the grain size but also permits pore-grain boundary separation.

If two small pores become one large pore, reduce the total surface area, and the total free energy of the system decreases. Similarly, when a pore passes through the interior of the grain to a grain boundary, free energy is required to move the boundary away from the pore. [27]

The coarsening of internal pores in grains can occur either by volume diffusion between pores or reattach to boundary and coarsening by the pores coalescence on it. During the grain growth, the internal pores are consequently reattached to a grain boundary. Reattachment is generally favored because the initially separated pores are likely to separate from the disappearing grain, the increasing driving force as show in Fig. 20. (A). [32] One form of internal pore is separated from the boundary of disappearing grain. As the pore separation from the boundaries of disappearing grains, the grain-boundary area decrease, thus decrease the mobility of grain boundary. The slow grain boundary mobility cause the grain growth which accompanies with the grain size increase and the pores reattach the boundary and coalescence again as show in Fig. 20. (B). In fact, the increasing of internal pore size is attributed to the grain growth. However, this assumption is established if the pore separated from a small disappearing grain is easier than the pore separated from a large grain.

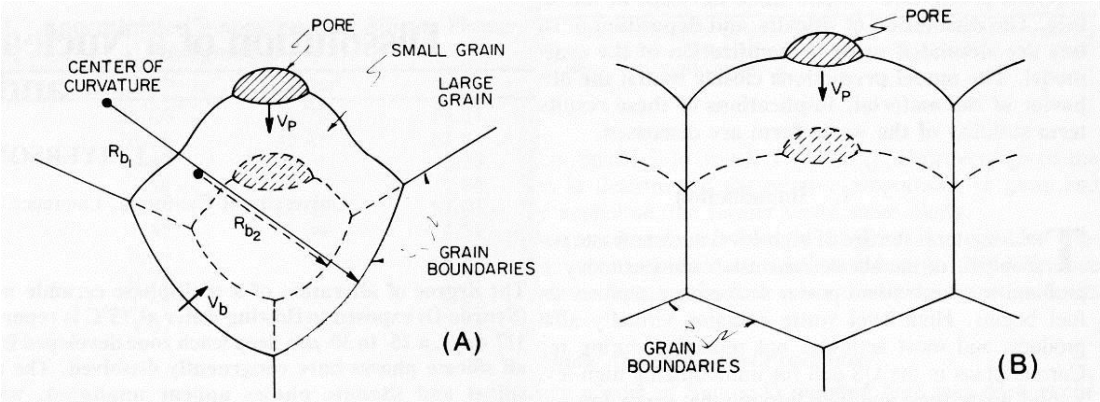

Fig. 20. Schematic illustrating motion of pores attached to (A) disappearing grain, and (B) growth grain.[32]

Sintering and coarsening both depend on the rate of atomic motion, as evident by similar activation energies. When heated, atoms randomly move from high energy, small grains to lower energy, larger grains. The large grains naturally consume the small grains. There are many factors influence coarsening event, such as solute segregation, pore attachment, precipitate or second phase drag, crystal orientation and liquid phase.

Pores not on grain boundaries become stable during sintering. Then the goal is to keep the pores coupled to the grain boundaries. A pinning force exists between the pore and the grain boundary, even when it is moving. The magnitude of the pinning force depends on the surface energy and pore shape. The dihedral angles and pore size determine the chance of pore separation from the boundary during sintering. Coalescence occurs when grains contact with near coincidence conditions, so after an initial transient a steady state dihedral angle emerges.[16]

Show densification depends on the grain-pore interaction. The pore shrink if there are local vacancy annihilation sites free surfaces or grain boundaries, yet at the same time neighboring pores interact and undergo coarsening by coalescence or diffusion through the solid vacancy flow or diffusion of a soluble atmosphere.[16][33]

The small pores will have more chance to be associated with the larger grain because of the natural affinity.

3.0 HYPHOTHESIS

Sintering can be divided into three stages.

Models for the initial stage of sintering

Most models describe the initial sintering stage involving interface formation and neck growth between primary particles with no grain growth. Based on the two-sphere model, a lot of densification equations were developed and different diffusion mechanisms were discussed. Only grain boundary diffusion and volume diffusion from grain boundary to neck area were considered to contribution on the densification. At this stage, the pore structure is open and fully interconnected. The shape of pores are not smooth and the pores occupied the grain boundary area.

Models for the intermediate stage of sintering

Start when grain growth begins and grain boundaries form extensively but pores are still connected with each other i.e. pore channel. The complex shape of the pore attend to continuous cylinder shape and the cylinder shape will shrink during the sintering. Most densification contribution is contributed in this stage.

Models for the final stage of sintering

As pores become pinched off and grain boundaries form a continuous network, the final stage of sintering starts. Thus, microstructure development according to the grain growth and grain coarsening mechanisms are very important during the final sintering.

There are two possible outcomes for the final stage:

1. When grain boundary mobility equal to the pore mobility. Pores are closed and become small nearly spherical shape, most of them located at grain boundaries where 3-grains or 4-grains corners.
2. When grain boundary mobility larger than pore mobility. The closed pores are mostly isolated within the grains.

In this stage, the density increase slightly but the grain growth rapidly. For the first one condition the pores remain attached to the grain boundary and move together with the grain boundary during grain growth, and pores will shrink at the end of the process. Alternatively, isolated pores located in the grains because the grain boundary mobility is too fast and breakaway from the pore leaving them isolated in the interior grain.

Pores are become stable in the grain during the sintering, it will tetrad the densification. Thus, apply energy to the grain boundary mobility can help pore reattach to the grain boundary. When prolong the sintering holding time, the moving grain boundary will drag the pore in grain repeatedly. The pores will have more chance to shrink when located on the grain boundary.

In real process, the sintering atmosphere influence sintering bonding and densification. It can be predicted that sintering in vacuum the grain size is smaller than the same condition in argon system. The pores can be eliminated during the final stage in the vacuum system; however, in atmosphere-based sintering, the pores which entrapped gas will grow and become stable while grain growth.

The pores with entrapped gas will not eliminate the pore numbers due to the pressure in the pore. Additionally, the gas trapped within the closed pores, giving the internal pressure. The internal gas which assuming idea gas behavior, increases with time or temperature that swelling the pore. It will resist the densification in the final stage sintering.

This work attempts to verify the above views, and to suggest that in certain metals where grain coarsening easily occurs the sintering process should be conducted in the temperature regime prior to grain growth, that is below the temperature of grain coarsening.

4.0 EXPERIMENTAL PROCEDURE

4.1 GREEN PARTS PREPARATION

4.1.1 Powder Characteristic

Metal additive manufacturing process are transforming the metal manufacturing industry, particularly in those areas where traditional manufacturing reach its limitation of freedom and flexibility.

The material used in this experiment is an austenitic 316L stainless steel. This material is a widely used steel because it offers superior corrosion resistance compared to both ferritic and martensitic grade. Type 316L contains a small amount of molybdenum for enhanced corrosion resistance [34].

The water-atomized stainless steel powders of 316L with three different particle sizes were used in this study. The mean particle size are 41µm, 24µm and 15µm, respectively.

Before any printing was performed, the powder was treated at 195°C for 8-10 hours to remove the water from as-received powder.

4.1.2 Printing

The samples for this study were printed using the M-Flex ExOne powder bed binder jet 3D printer, shown in Fig. 21. This is an additive manufacturing system which provides high design freedom and complex geometries without need of tooling. This binder jetting process is economical and creates functional parts with large load, faster speed and no support structure. Furthermore, various industry grade materials can be printed by this system, such as ceramics, stainless steel, bronze, iron and tungsten etc.

This system has a 400mm x 250mm x250mm build volume inside a powder box and the build speed can achieve 30-60 seconds per layer.[35] M-Flex 3D printer has four parts: powder box, spreading part, binder part and software part. The powder box is a container with a mobile plate inside which can moved up and down.

The powder spreading part contains: a hopper where powders are load in, a recoater with a roller can spread powder into a thin layer and a heating system can dry the powder. The binder parts have a printhead consist of binder supply system and cleaner system which spray binder into the powder layer while printing, and swipe the printhead for cleaning at the cleaning zone.[36]

The setting parameter in this thesis is: recoated speed of 130 mm/s, oscillator speed of 2050 rpm, roller speed of 250 rpm, roller traverse speed of 15 mm/s, drying speed of 17 mm/s and the coupon parameter is 0.5x0.5x0.2 inches.

Fig. 21. M-Flex powder bed binder jet 3D Printer.

First, sent the digital model file to the 3D printer. Then, print layer by layer following a 2D thickness powder particles bonded with liquid binder to formed an object. Before printing, the powder box needs to be engaged in the system and several foundation layers are spread and pre-heated for the parts building up.

The printing process can be divided into four steps: print 2D pattern, dry the binder, lower powder box and spread a new powder layer. Fig. 22. (a)-(c) show a cycle of printing one layer. In Fig. 22. (a) the printhead print the 2D pattern of product cross-section on the powder bed by using binder agent. During drying step, shows in Fig. 22. (b), the water in the binder will evaporate and the remaining polymer will form a thin film to bond with particles together. After drying, the powder bed lower a layer and the powder can be load and spread by the roller in a new layer, shows in Fig. 22. (c) These steps will run as a cycle to build layer by layer until the product is finished.

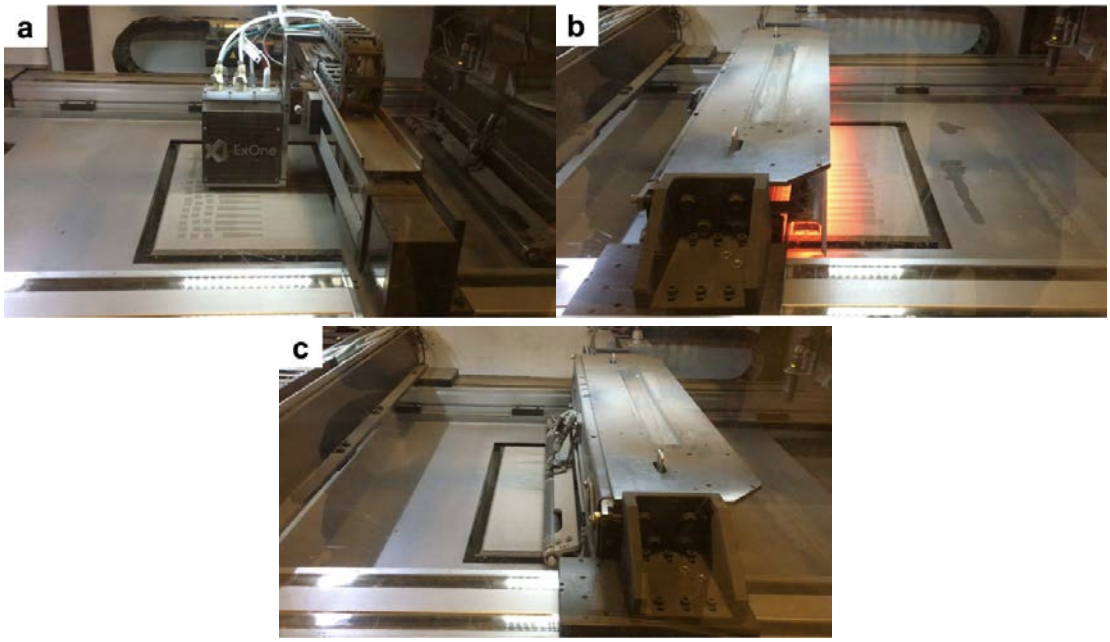

Fig. 22. Binder jetting 3D printing process: (a) printing 2D pattern by using binder (b) binder drying (c) spreading a powder layer.

After the product is rinted, powder bed is lowered to the bottom of the powder box. Then, the powder box is transferred to the curing furnace. The samples are cured at 195°C for 8 hours to remove the binder. The curing furnace is shown in Fig. 23. This step increases the strength of the printed samples so they can be picked up from the powder bed easily. The surrounding powders assure prevention of the green parts to get distorted during the curing stage. After the samples are picked up from powder box, shows in Fig. 24, they are ready for sintering and it is also the green parts resulting in the final product.

Fig. 23. Curing furnace.

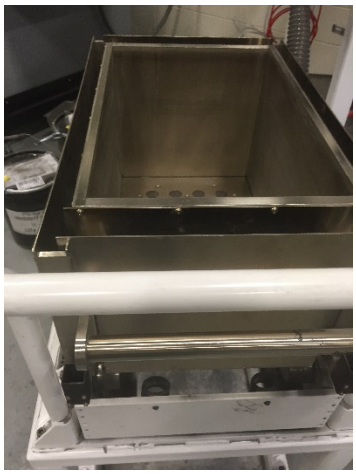

Fig. 24. Powder box.

4.2 SINTERING PROCESS

After curing, the samples are ready for the sintering process to get the high densification. The sintering stage that was discussed in Section. 2.2, shows the importance of temperature ratio in densification during sintering. The analysis of sintering parameters is determined with densification, porosity and pores shape control. During the sintering, samples are in a 96% Argon + 4% Hydrogen atmosphere to prevent the oxidation.

The sintering temperature T_S in this research was been chosen based on the following approximation:

$$0.91 \leq \frac{T_S}{T_M} \leq 0.99 \qquad (20)$$

where T_M is the melting temperature.

Table. 1. shows the chemical composition of the 316L stainless steel. Based on JMatPro analysis, shows in Fig. 25., the melting temperature of the 316L stainless steel is 1413.87°C.

Table. 1. Chemical composition of standard 316L stainless steel.

	Chemical Composition (wt.%)									
Elements	Fe	Cr	Ni	Mo	Mn	Si	N	P	C	S
Standard 316L	Bal.	18	14	3	2	1	1	0.045	0.03	0.03

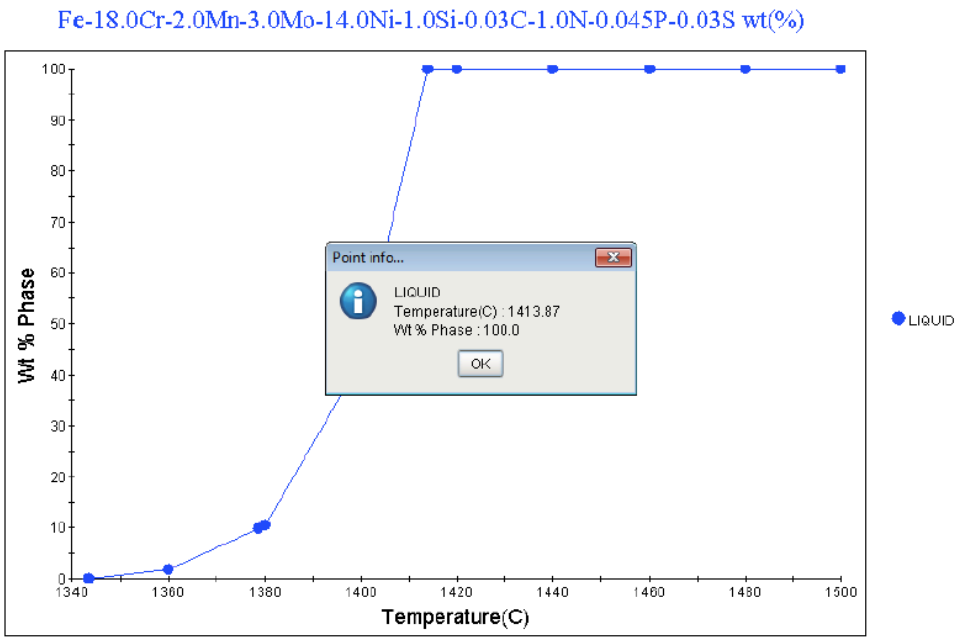

Fig. 25. Melting temperature of the standard 316L stainless steel by JMatPro.

Based on the melting temperature and the Eq.(20) the sintering parameters are designed as

Table. 2. shows below.

Table. 2. Sintering temperature and time parameters design for standard 316L.

Standard 316L		
Sintering temperature T_S (°C)	T_S/T_M (K)	Sintering holding time (mins)
1300	0.91	90
		360
		1440
1356	0.97	90
		360
		1440
1380	0.98	90
		360

In this research, five steps of sintering parameters were designed as below, and plotted in Fig. 26.

1. Raise the temperature from room temperature (25°C) to 350°C at a heating rate of 5°C/min.
2. Hold the temperature at 350°C for 120 mins.

3. Raise the temperature from 350°C to 420°C at a heating rate of 5°C/min.

4. Hold the temperature at 420°C for 30 mins.

5. Raise the temperature from 420°C to 630°C at a heating rate of 5°C/min.

6. Hold the temperature at 630°C for 30 mins.

7. Raise the temperature from 630°C to 1000°C at a heating rate of 5°C/min.

8. Continue raise the temperature from 1000°C to desired temperature at a heating rate of 1°C/min.

9. Hold the temperature at the desired temperature for desired time.

10. Cool down to 1000°C at a cooling rate of 1°C/min.

11. Continue cool down to room temperature at a cooling rate of 3°C/min.

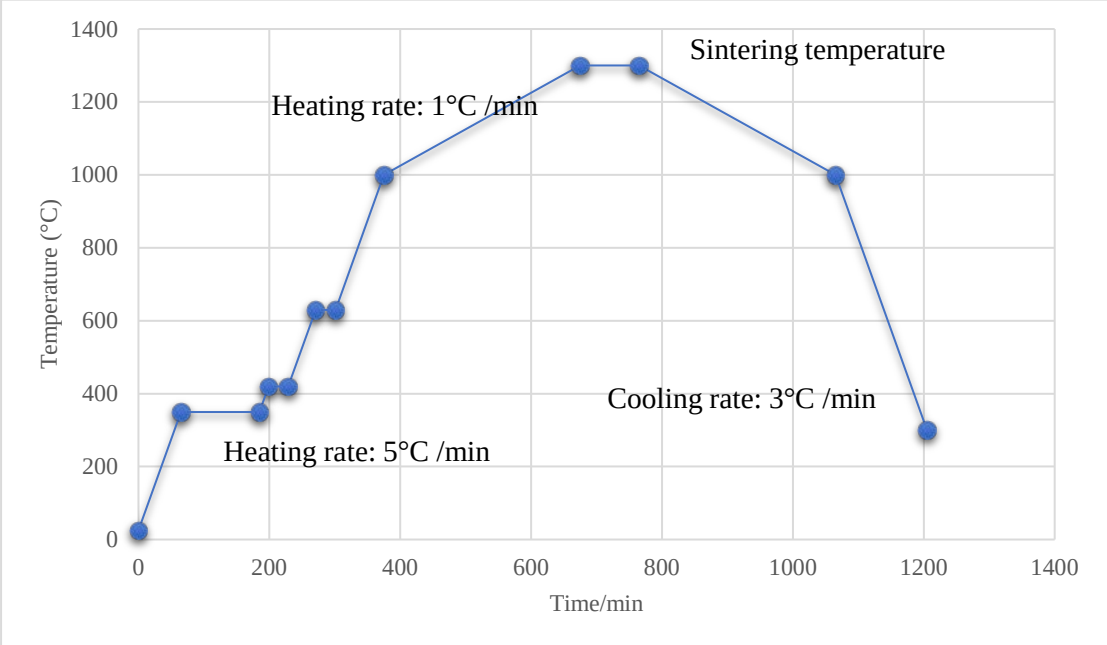

Fig. 26. Sintering process steps example for 316L stainless steel sintering at 1356°C for 90 mins.

For the vacuum sintering

Because the green specimens after printed is very friable, they need some strength before put into the quartz tube. The green specimens are pre-sintering at 600°C for 60mins and furnace cool to room temperature. After pre-sintering, the specimen is vacuum sintering in the sealing quartz tube. Then the same sintering process is adopted as that in the argon gas.

4.3 DENSITY MEASUREMENT

The Archimedes technique was applied to measure the density for each coupon. Because the porous sample has surface-opened pores, use the ASTM B962 standard method to measure surface-connected porosity. First, weighted the sample in air, then slight waterproof glue is used to seal the surface and the specimen is reweighed. Second, the test specimen is weighed when immersed in water and its density calculated based on Archimedes' principle[37].

The specimen support for weighing in water is shown in Fig. 27. Take care to ensure that the wire does not restrict the free movement of the specimen and does not touch the container. The water should cover any wire twists and the specimen. To obtain the most precise density, it was measured independently three times using electric balance with ±1mg accuracy. The calculation of density ρ follows Eq. (21) below, where ρ_W is the density of water [38].

$$\rho = \frac{A \times \rho_W}{B - (C - A + D)} \qquad (21)$$

where A is the mass of the sintered part without glue in air, B is the mass of part with glue in the water, C is the mass of part with glue in air and D is the mass of support part in water.

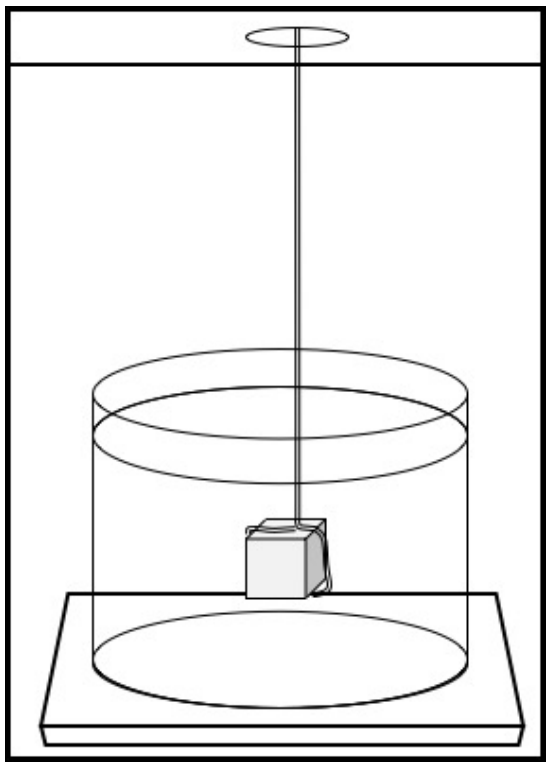

Fig. 27. Archimedes methods for holding the test specimen when weighing in water.

4.4 MICROSTRUCTURE ANALYSIS

4.4.1 Optical Microstructure Analysis

Samples were cut by diamond saw, and were mounted in Bakelite. The mounted samples were ground using SiC grinding paper and polished using 0.05μm Al_2O_3 with deionized water. Before etching, observed the pores distribution was analyzed under the optical microscope. Because there are a lot of etching pit appeared after being etched, it is hard to distinguish pores and etching pits under optical microscope.

4.4.2 Etching for OM Analysis

The polished samples were electrochemically etched in 10% oxalic acid. After applying the etching etched surfaces were rinsed with deionized water and alcohol and then dried. The microstructure analysis was made by optical microscope and scanning electron microscopy (SEM) using JEOL JEM-6510 electron microscope.

4.5 GRAIN SIZE MEASUREMENT

The grain size measurement was performed by image software, ImageJ, using the liner interception method (ASTM E112).[39] Instead of micrographs put the approximated number of grains. The measurements were done on 3 micrographs at 500X magnification and on each micrograph 5-7 lines oriented in various directions were considered.

4.6 FRATAL DIMENSION ANALYSIS

The fractal dimension concept was first introduced by B.B Mandelbrot in 1973.[40] A fractal dimension is an index for characterizing pattern by qualifying their complexity as a ratio the change of detail to the change of scale. It is a method that can qualify the geometry of irregular shape.

The fractal theory can well describe the disorder and irregular shape performance of porous material. H.P. Tang[41] has used the fractal theory in the research of the pore structure of stainless steel.

A two-dimensional object can be divided into $N(\varepsilon)$ small squares and each of them is measured by the length ε. Therefore, the fractal dimension D can be calculated as:

$$D = \frac{\ln N(\varepsilon)}{\ln \varepsilon} \qquad (22)$$

In this research, the fractal dimensions were determined using the box counting method which has been proven to have higher calculation speed and higher accuracy by Dougan[42] and Shi[43].

To determine the pore shape distribution and porosity from OM images of the microstructure can use this method. By using the ImageJ program, one can transform

the OM picture to binary image, and start calculate the area of pores. The fractal dimension *D* and standard deviation of porosity can be calculated by box counting method. The process is show in Fig. 28.

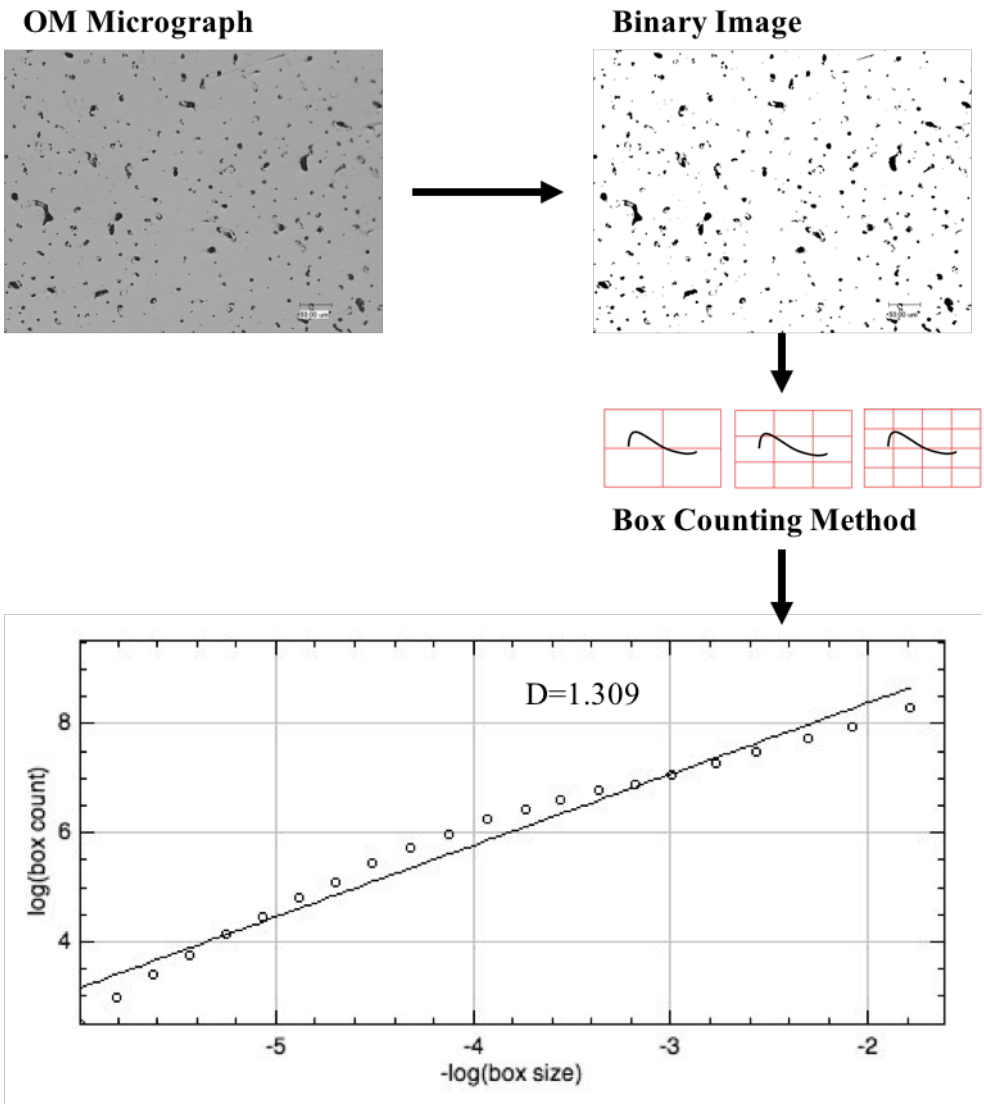

Fig. 28. Calculation of fractal dimensions with box-counting method.

5.0 RESULTS AND DISCUSSION

5.1 DENSIFICATION RESPONSE

In this section, the density for each sample is calculated based on Archimedes method and the OM images are taken to see the internal microstructure change. Area porosity obtained through the OM images are compared to the body porosity to show the mechanisms of pore-migration during sintering. Based on the Eq.(21), the density ρ can be calculated by as follow:

$$\rho = \frac{A \times \rho_W}{B - (C - A + D)} \quad (21)$$

Since the theoretical density of 316L stainless steel is known as 8.00g/cm^3, the densification can be calculated as:

$$Densification = \frac{\rho}{8} \times 100\% \quad (23)$$

The densification of the sintered samples are listed in Table. 3.

Table. 3 316L stainless steel different particle size densification.

Densification	Temperature (ºC)			
Particle size (μm)	1300	1356	1366	1380
41	68.41%	82.00%	83.00%	84.38%
24	69.13%	82.13%	82.75%	76.88%
15	73.89%	92.35%	90.54%	80.00%

5.2 EFFECT OF SINTERING TEMPERATURE

Fig. 29. shows the densification at different temperature for different particle size sample sintered in 96% argon + 4% Hydrogen. From the results for the standard 316L stainless steel, the highest density 92.35% appeared at 1356ºC for particle size 15μm. Overall, the finer particle size attributed to a higher final densification.

According to the sintering theory[9][10][14], the final density increase with the increasing sintering temperature. However, in Fig. 29, the curve decrease at 1380ºC which means after 1356ºC increasing the temperature does not improve densification.

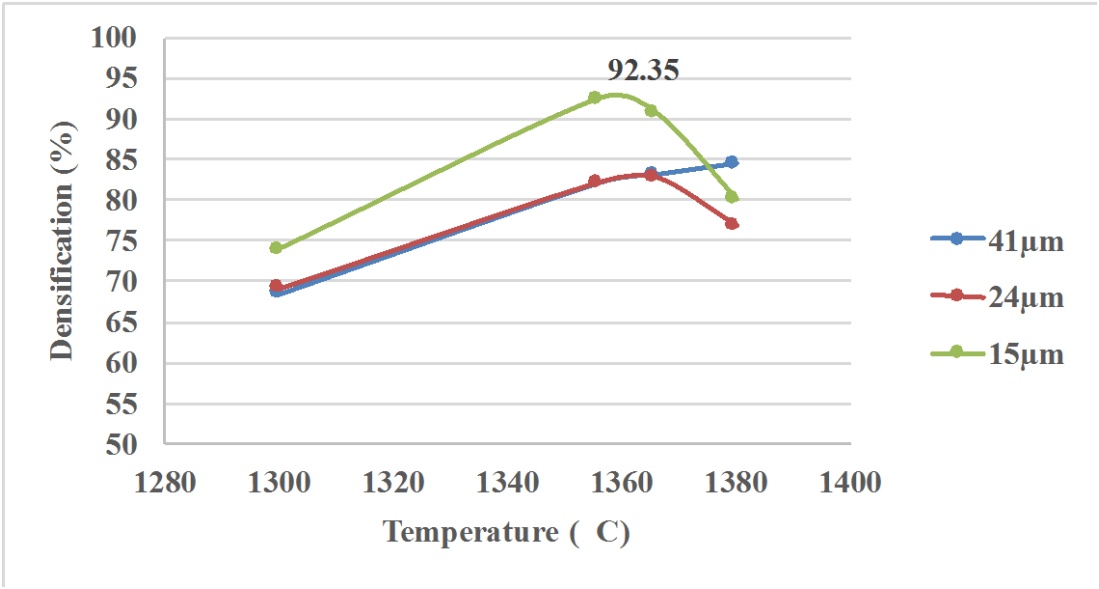

Fig. 29. Densification (%) versus temperature (ºC)

To investigate the reasons why density decreas, the microstructure evolution of the particle size 15µm is given as an example in Fig. 30. (a-d). From Fig. 30. (a), a lot of large pores attached to the grain boundary and 3-grains edge. When the pores are attached to the grain boundaries, grain boundary diffusion is the main transport mechanism.

However, in Fig. 30. (b) the figure indicates pore-boundary separation, most of the pore are small and isolated in the grains. The system energy is lower when pore located at grain boundary; when pore and the boundary are separated, the system energy is increased because of newly created interfacial area.

When continuing increase the temperature, in Fig. 30. (d), the pore become larger and appeared on the grain boundary again. The number of the pores does not decrease, and the pore size is increased. As discussed before, when sintering at high temperature the densification will be slower at the final stage due to the isolated pores within the grains. When the pore is isolated within the grains, the main diffusion mechanism change from grain boundary diffusion to volume diffusion which is very slow. Thus, the isolated pores in grains will limit the densification process.

As shown in Fig. 30. (d), most pores are isolated in grains and some are reattached to the grain boundary which is the evidence of grain boundary mobility is too high at this condition. In fact, it will never get the full density when sintering at a temperature higher than 1356 ºC due to the pore-boundary separation and isolated pores can not be eliminated.

From Fig. 30., another interesting thing is there are lots of twin boundaries appeared in the 1356 ºC and 1366 ºC, since twin boundaries attribute good effect on mechanical properties[44]. Small amount of twin boundaries appeared in the 1356 ºC as shown in Fig. 30 (b). When increased to 1366 ºC, large number of twin boundaries appeared as shown in Fig. (c). However, when the temperature was increased to 1380ºC,

the twin boundaries disappeared. According to the grain growth theory related to annealing twins[45][48], a twin boundary forms due to a stacking fault during grain growth. Grain growth is a process of reducing the interface energy, and the twin boundaries have a lower energy. Which means when grain stop growth the twin boundaries disappear. It can be corresponded to the reason that the swelling pore retarded grain growth, as show in Fig. 30. (d).

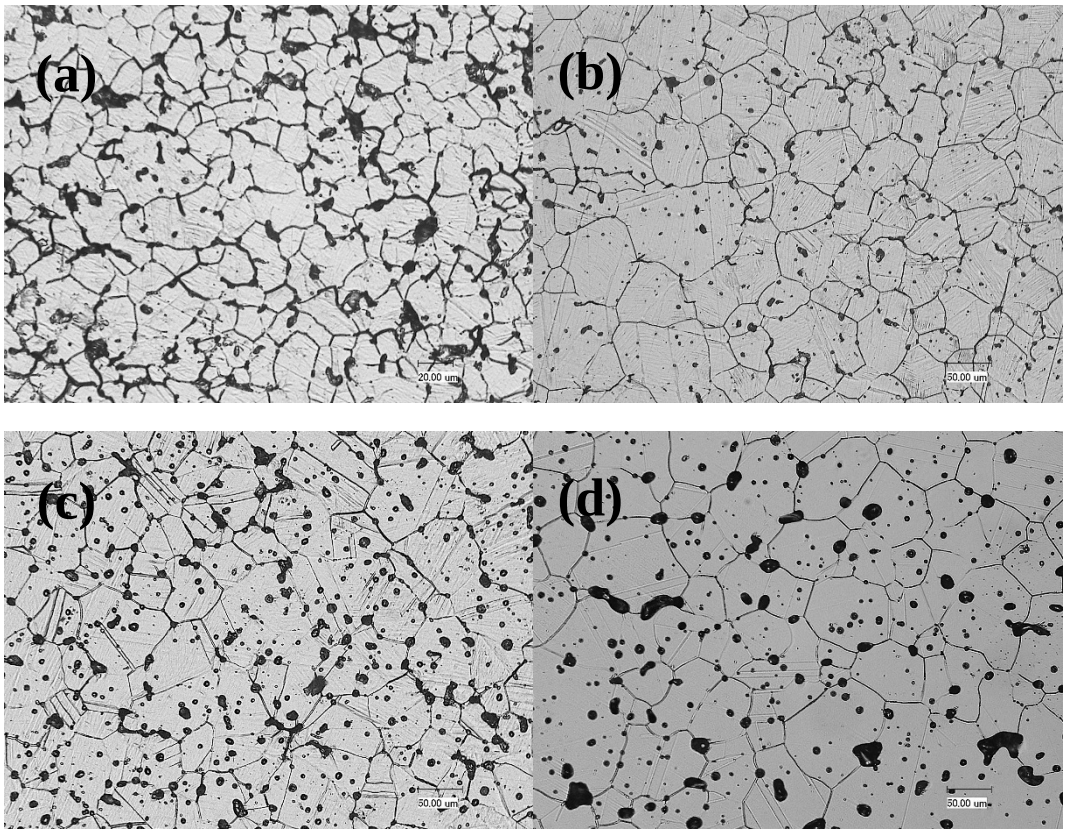

Fig. 30. Optical micrographs of the 316L stainless steel (particle size 15μm) sintered at (a) 1300 ºC, (b) 1356 ºC, (c) 1366 ºC and (d)1380 ºC for 90 mins sintering in argon.

During sintering, there are three possible interactions between pores and grain boundaries have three possible: the pore attached on grain boundary and retarded grain growth, the pore is dragged by the moving grain boundary during grain growth or the grain boundary mobility faster than pore mobility and breakaway from pore. Fig. 31. shows the process of grain growth versus densification and the schematic of pores migration.

The first three schematics show the process of pore from grain boundary to internal grain with the grain growth. The last schematic shows the swelling pore and stop grain growth.

As described in section 2.2.2 [33], when sintering in vacuum the pores can be eliminated during final stage. However, in atmosphere-based sintering, the entrapped gas pores grow and become stable when grain growth continually. Pore swelling due to pressure in the pore decreases as it enlarges.

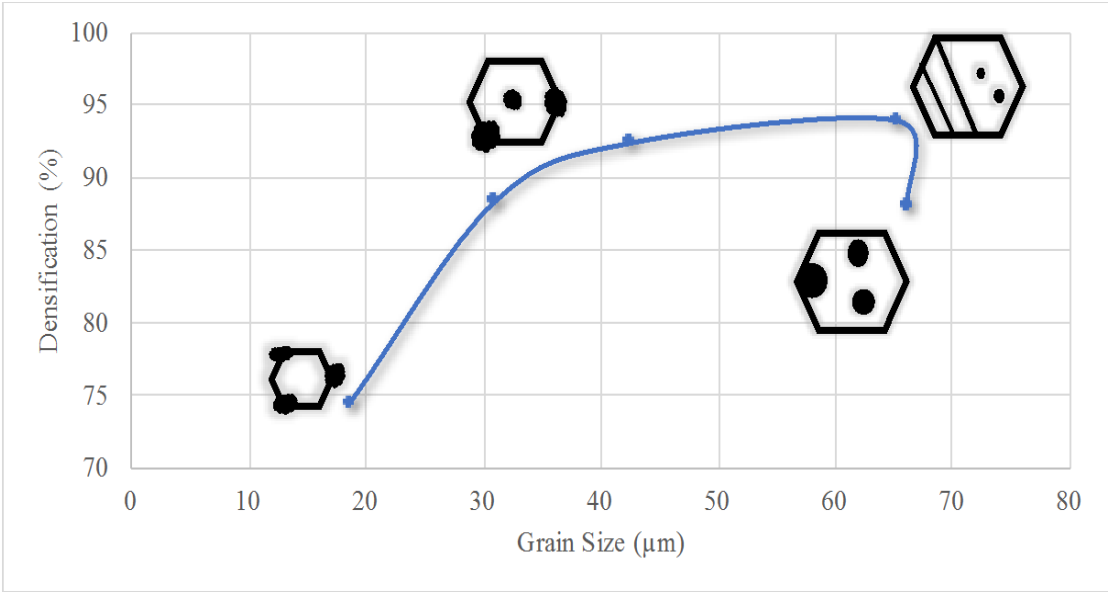

Fig. 31. Schematic of sintering behavior for 316L stainless steel with particle size 15µm showing the grain size versus densification and the schematic of pores migration.

The grain growth model that links the characteristic grain size G to the sintering holding time t shows as follow:[16]

$$G^3 = {G_0}^3 + Kt \qquad (24)$$

where G is grain size, G_0 is a starting grain size, t is time and K is the grain growth rate parameter.

The grain growth parameter related to the grain boundary mobility *K* is expressed as:

$$K = K_0 + exp\left(-\frac{Q_B}{RT}\right) \quad (25)$$

where K_0 is the frequency factor, Q_B is the activation energy, *R* is the universal gas constant and *T* is the absolute temperature.

During sintering, the ideal relationship between grain size and temperature can be calculated as follow:

Combine Eq. (24) and (25) $$G^3 = {G_0}^3 + exp\left(-\frac{Q_B}{RT}\right)t \quad (26)$$

Fittings of the experimental results plotted according to the Eq. (26) are show in Fig. 32. It can be seen that over 1630K, the grain size is larger than the idea size. Too large grain size is a reason that we cannot reach higher temperature. Thus, choose the temperature and controlled the grain size at correspond size can reach the full density.

According to the Eq. (26), the relationship between grain size and temperature will influence by sintering time *t*, Fig. shows different sintering holding time influence on grain size and temperature. As seen in Fig. 33. grain size increases with the temperature increases. Grain size of the samples sintering for longer holding time were found to be always larger grain size than the 90mins.

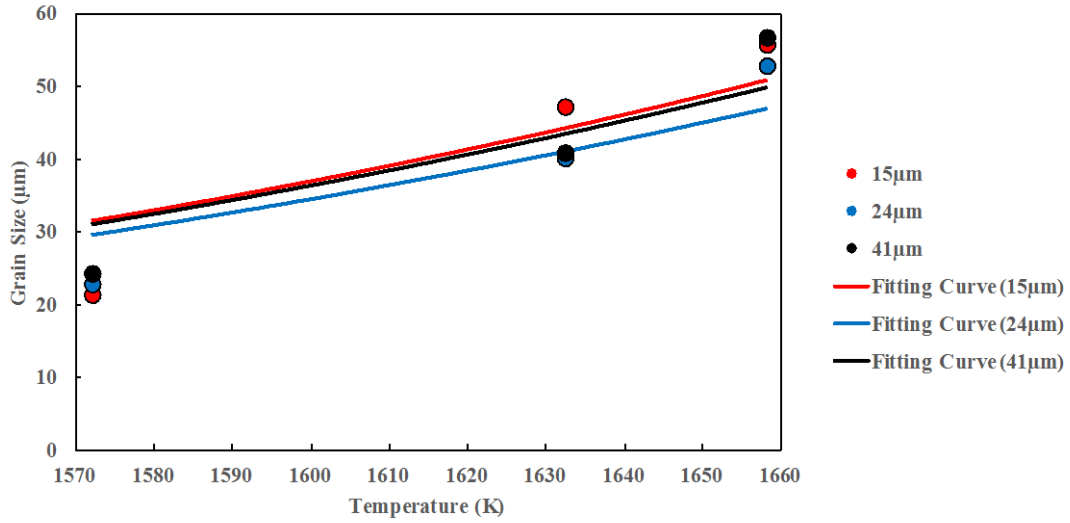

Fig. 32. Sintering data for 316L stainless steel shows the grain size versus temperature.

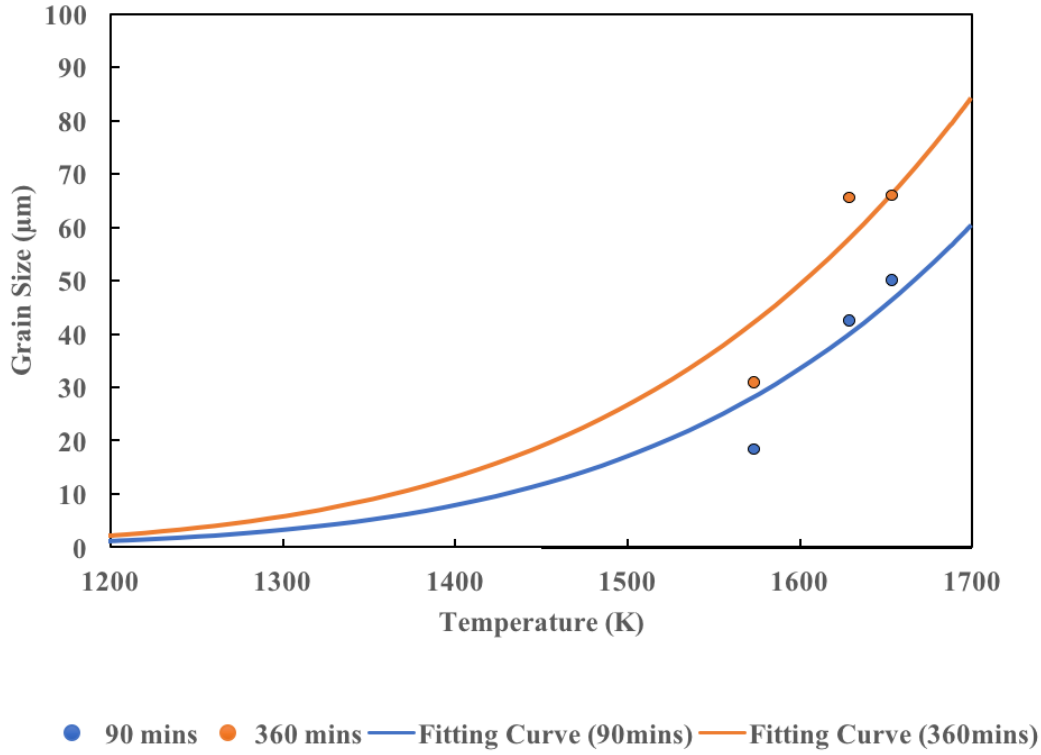

Fig. 33. Grain size versus temperature of sintering 316L stainless steel 15µm for different holding time.

The microstructure shows a progression from irregular shape approaches to spherical shape when increasing degree of sintering apparently. Fig. 34. shows curves of specimen densification and pores fractal dimension varied with sintering temperature. The specimen densification increases with pore fractal dimension decrease wholly. It qualified that the pore shape from irregular to rounded. The fractal dimension has an increase at 1380 ºC, it is because the pore coarsening and reattach to the grain boundary which increase the average dimension of pores.[47]

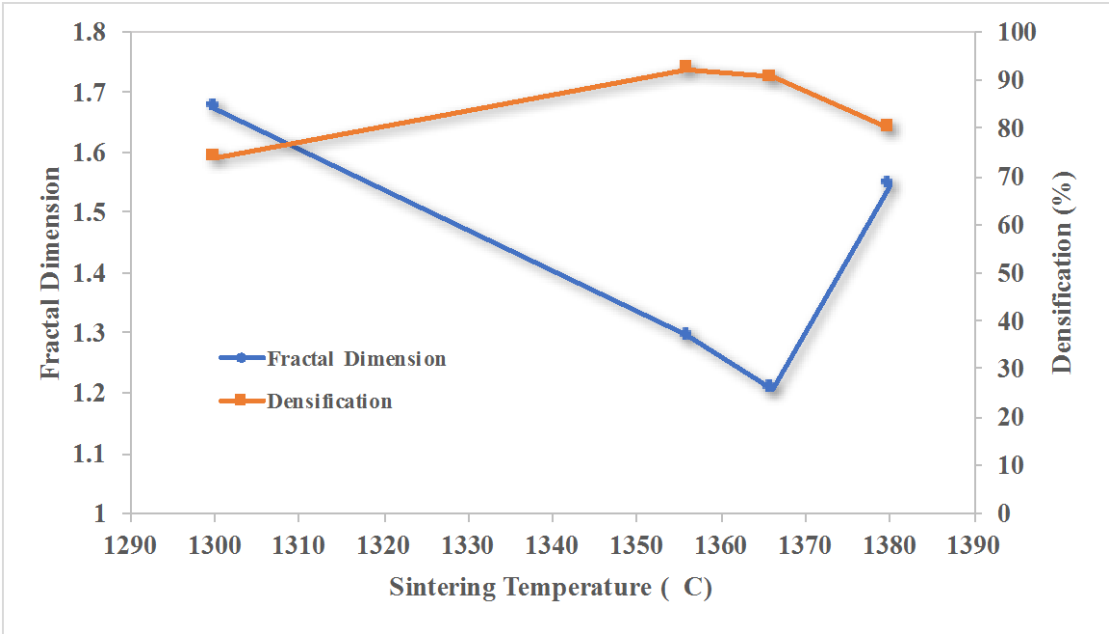

Fig. 34. Variations of density and pores fractal dimension with sintering temperature.

5.3 EFFECT OF SINTERING HOLDING TIME

Several factors can affect final pore elimination, increase holding time on sintering temperature is an important factor that will cause pore coalescence and small pore disappear[9][16]. The effect of sintering time on the final density can be explained by the following equation:[48]

$$F_s = f_I + B_0 exp\left(-\frac{Q}{kT}\right)\ln(t) \quad (27)$$

Where F_s is the sintered fractional density, f_I is the fractional density at the beginning of the intermediate stage, *k* is the Boltzmann's constants, *T* is the absolute temperature, B_0 is a collection of constant that depend on surface energies, atomic size etc. and *t* is the time. As the temperature reach a high level, small temperature changes can have large effect, while the time effect is smaller.

From Table. 4. and Fig. 35. the specimens sintering at 1300 ºC in argon, densification increasing with the holding time increasing. The highest density shows in 1356 ºC holding for 360mins. However, the densification does not change at 1356 ºC when increasing the holding time. As shows in Fig. 35., the densification data at 1356 ºC are all higher than 1300 ºC. But, the 1300 ºC curve is still arising and the 1356 ºC

curve is remain stable. For the 1380 ºC, as discuss in section 5.2 the temperature is too high and can not reach the full density. Thus, there are some reasons limit the densification for 1356 ºC. On the other hand, if continually prolonged the holding time at 1300 ºC may reach higher densification.

Table. 4. The densification of stainless steel 15µm with different holding time on different sintering temperature.

Densification	Holing time at sintering temperature (mins)		
Temperature (ºC)	90	360	1440
1300	73.89%	74.38%	88.34%
1356	92.35%	93.90%	92.21%
1380	80.00%	88.10%	

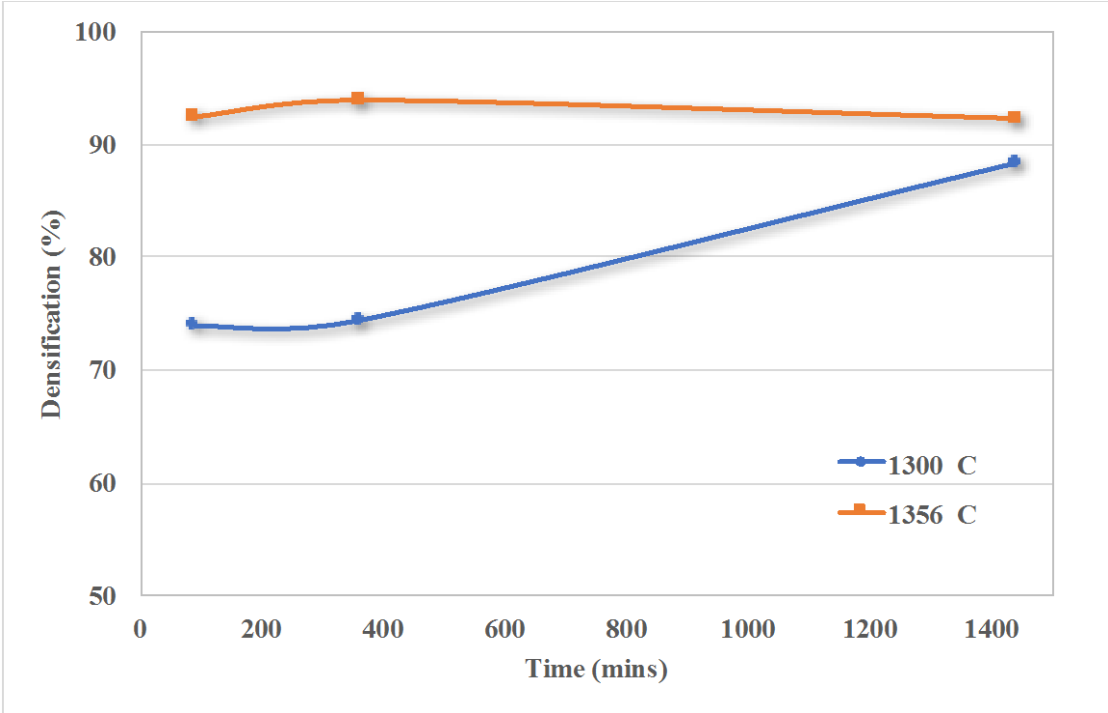

Fig. 35. Densification versus holding time at different sintering temperature for 316L stainless steel 15µm.

Fig. 36. (d)-(f) show the microstructure of the 316L stainless steel 15μm specimens sintered for 90mins, 360mins and 24hrs at 1300 ºC in argon. At this low temperature, Fig. 36. (d) has larger pores area than high temperature Fig. 36. (a), and most of pores are located at grain boundary in faceted-shape. Increasing the holding time to 360mins, as show in Fig. 36. (e), some pores breakaway from grain boundary. Continually increased the holding time, as show in Fig. 36. (f), grain size increased and pore numbers decreased which contributed to the increasing of densification, shows in Fig. 37.

Fig. 36. (a)-(c) show the microstructure of the 316L stainless steel 15μm specimens sintered for 90mins, 360mins and 24hrs at 1356 ºC. At this higher sintering temperature, most of the pores are isolated in the grains, as shows in Fig. 36. (a).

When increasing 4 times of the holding time to 360mins the densification only slight increase. However, prolonging 16 times of the holding time to 1440mins, the densification is not change. As show in Fig. 36. (c), the pores are coarsening and the number of pores are not decrease which cause the density decrease.

In the higher sintering temperature condition, during final stage the pores are left behind and remain in grains. The specimens which contained isolated pores have shown

that pore coarsening occurs by Ostwald ripening and a coalescence mechanism in the previous study.[17][22][25][23][26] The isolated pores entrapped with gas will prevent the full density.[17][19]

Fig. 36. (d) doesn't shows the twin boundaries. As the holding time increases to 360 mins, large number of twin boundaries appear as show in Fig. 36. (e). However, the amount of twin boundaries decrease when continually increase the holding time to 1440 mins, as shown in Fig. 36. (f). The grains grow as the holding time increases, shows in Fig., and the twin boundaries appear to reduce the interfacial energy initially. When the grain growth large enough, the twin boundaries will disappear due to the grain size become very large and grain boundaries disappear.

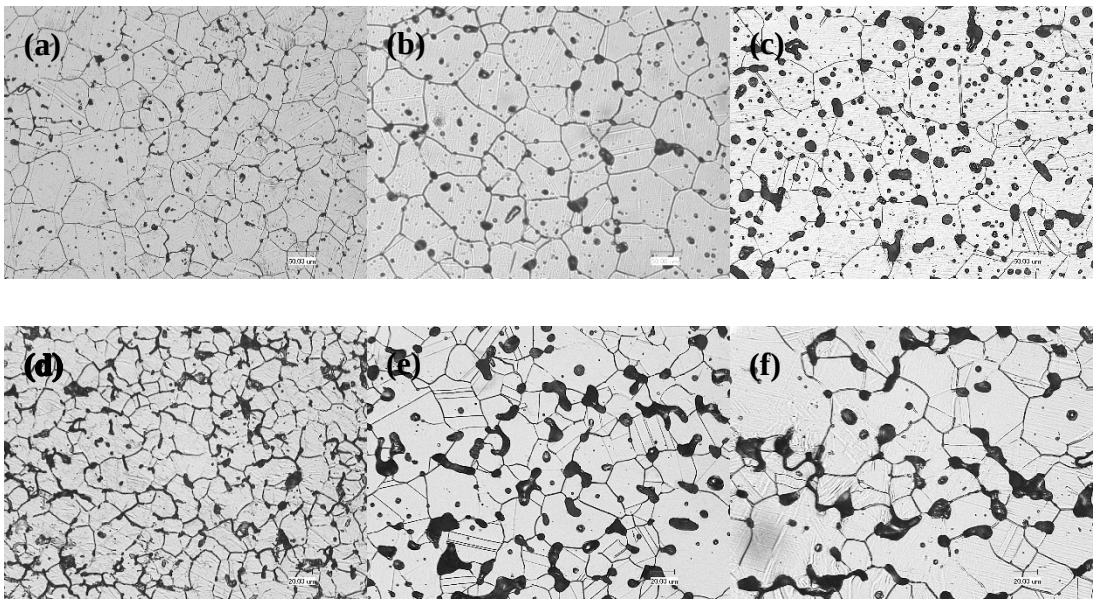

Fig. 36. Optical micrographs of the 316L stainless steel (particle size 15μm) sintered at 1356 ºC for (a) 90mins, (b) 360mins and (c) 24hrs. Sintered at 1300 ºC for (d) 90mins, (e) 360mins and (f) 24hrs in argon.

Prolong the holding time cause the rate of grain growth increase to a point that grain boundary breakaway from the pore. In Fig. 37. 1300 ºC shows the curve keep increase, grain growth during increasing time which is the evidence that grain boundary still can move and pores will be eliminated.

On the other hand, in 1356 ºC the curve remains stable after 360mins. It is because the pore retarded the grain growth. Compare to Fig. 38., the pores density also increased at 1356 ºC when prolong holding time to 1440 mins. All of these indicate prolong sintering time at 1356 ºC will not get higher density and even cause pore density increased.

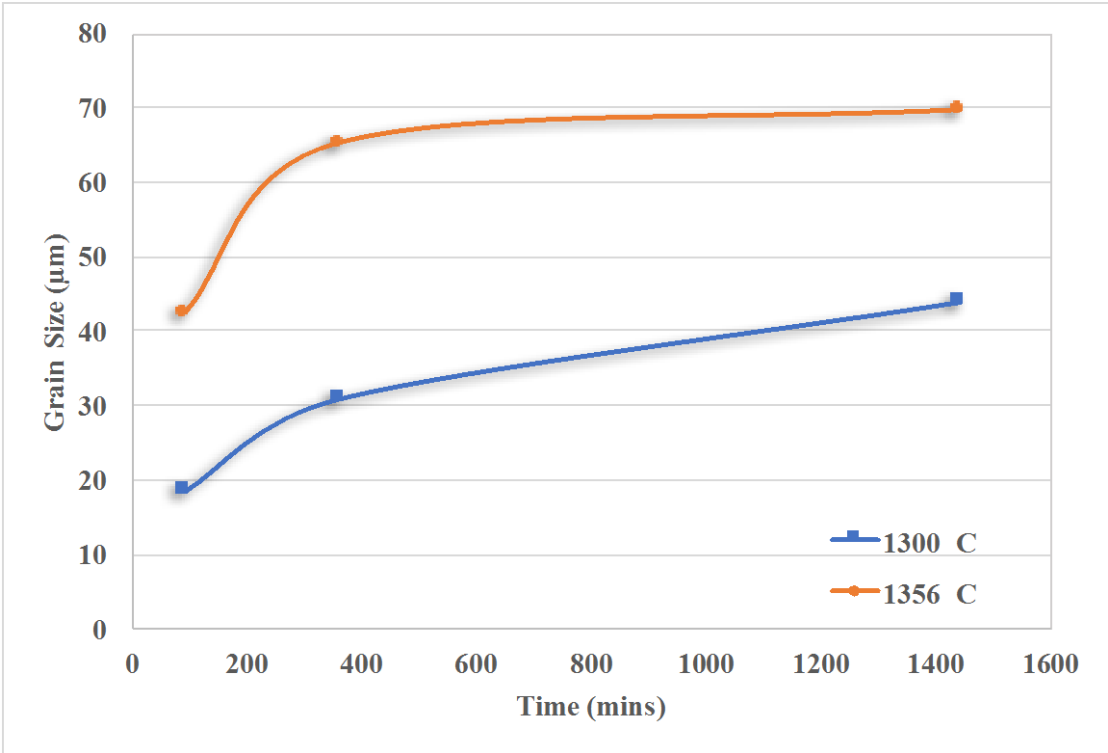

Fig. 37. Grain size versus holding time at the different sintering temperature for 316L stainless steel 15µm.

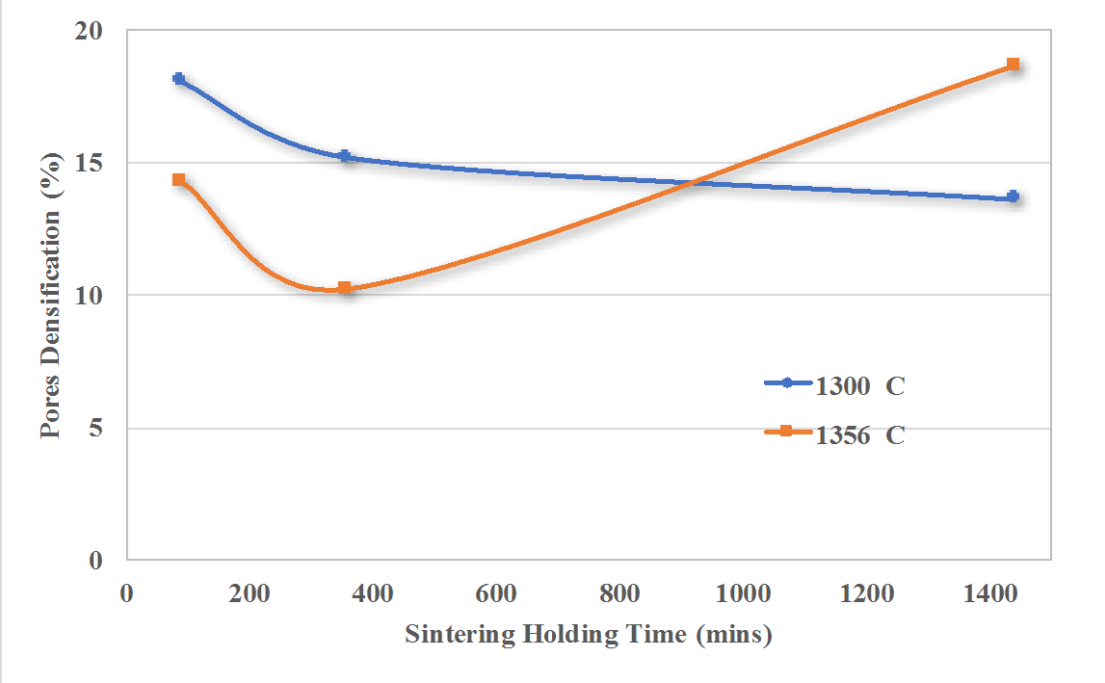

Fig. 38. Relationship between pores density and holding time at different temperatures.

Fig. 39. shows curves of specimen densification and pores fractal dimension varied with holding time at 1300 ºC. In this low temperature condition, the specimen densification increases with pore fractal dimension decrease. As show in Fig, pore shape from irregular approached spherical during the increasing holding time which decreasing the fractal dimension.

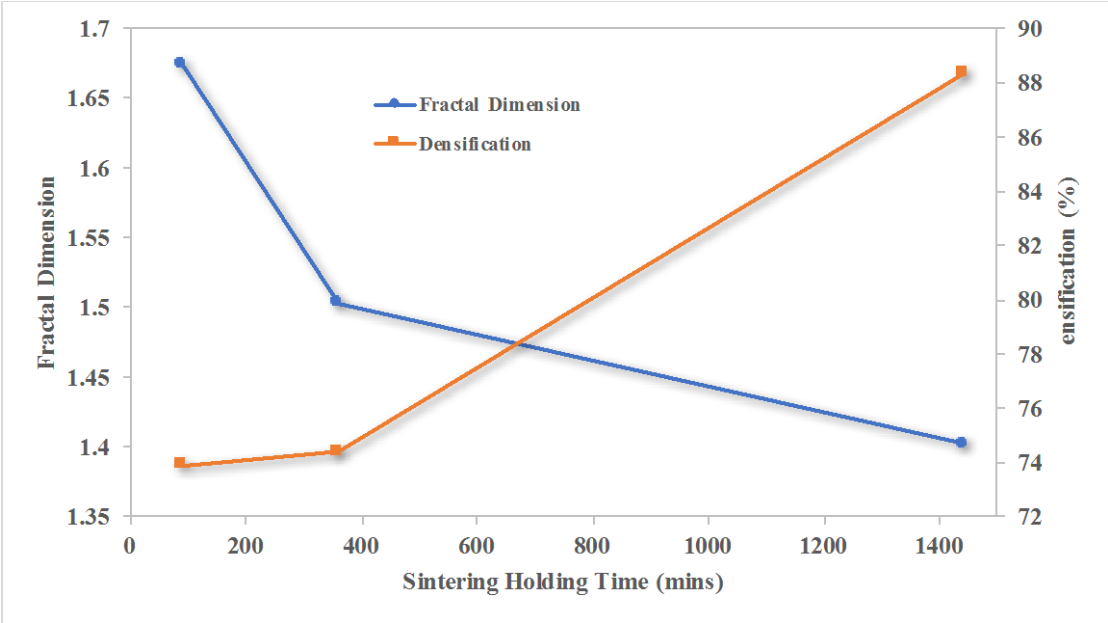

Fig. 39. Variations of density and pores fractal dimension with holding time.

The grain growth kinetics was studies base on Coble's model. For the systems containing mobile pores and in which grain boundary migration controlled by pores, the rate for the final stage sintering is expressed as:[49][50]

$$\frac{dG}{dt} = \frac{kD}{TG^n(1-\rho)^m} \qquad (28)$$

where G is grain size, ρ is relative density, t is time, T is the absolute temperature and k is a constant related to the material and grain growth mechanism.

For lattice diffusion controlled pore drag: $D=D_L$, n=2 and m=1. For surface diffusion controlled pore drag: $D=D_S$, n=3 and m=4/3. Integrating Eq. (28) gives:[51][52]

Lattice diffusion $$G^3 = \frac{k_1 D_L}{T\rho} t \quad (29)$$

Surface diffusion $$G^4 = \frac{k_2 D_S}{T(1-\rho)^{4/3}} t \quad (30)$$

where k_1 and k_2 are constants related to the material and grain growth mechanism.

Fittings of the experimental results plotted according to the Eq. (29) and Eq. (30) are show in Fig. 40. The grain growth mechanism was identified by comparing the correlation coefficient R^2. A correlation coefficient of 1 would be an ideal fit to the corresponding mechanism. It can be seen that a correlation coefficient close to 1, and thus a good linear fit was observed for the lattice diffusion controlled grain growth when sintering for 90 mins and surface diffusion controlled grain growth when sintering for 360mins.

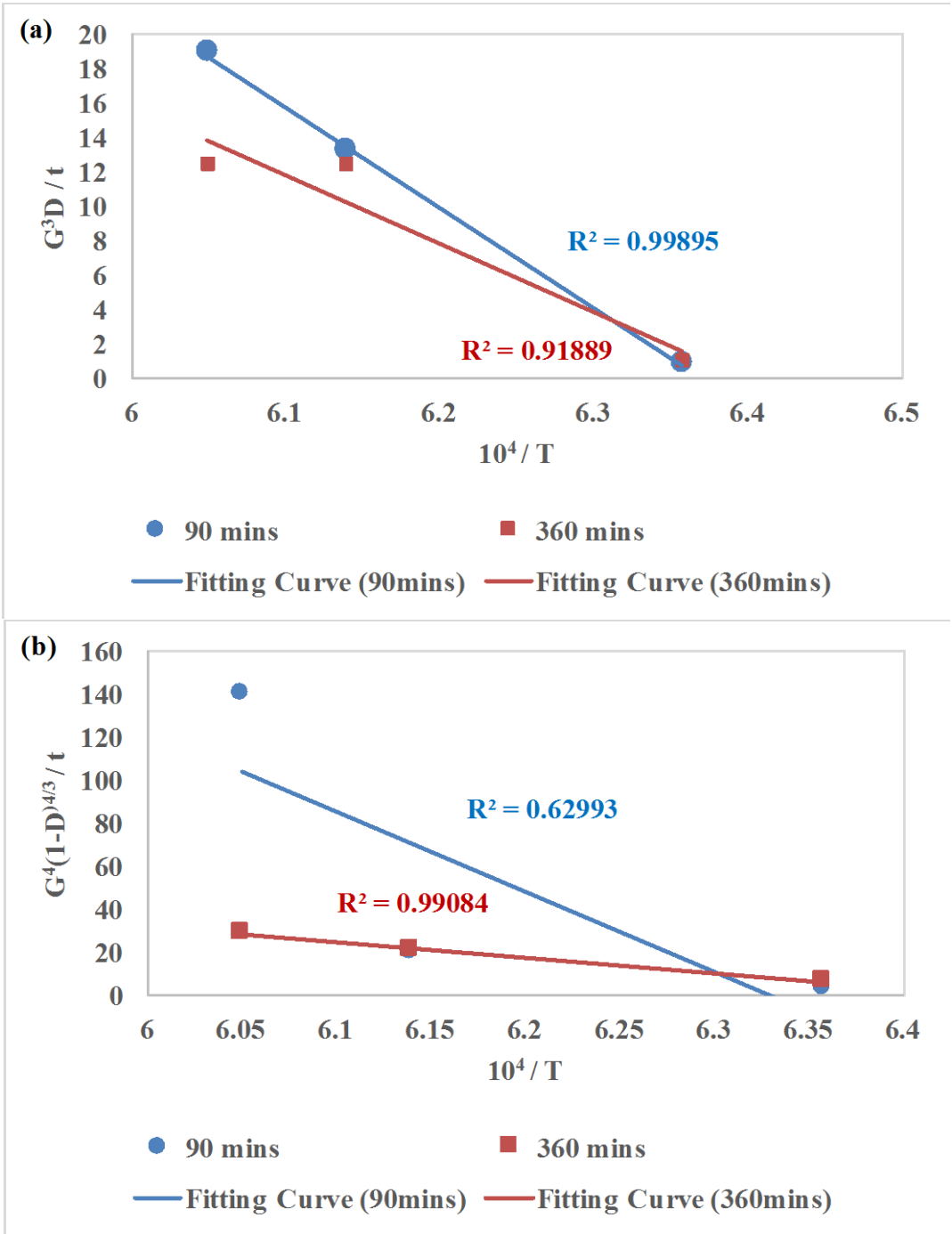

Fig. 40. 316L stainless steel 15μm grain growth data of microstructures fitted according to: (a) Coble's model of lattice diffusion-controlled pore drag and (b) Coble's model of surface diffusion-controlled pore drag.

Coble's model assumed concentric sphere diffusion model; however, Kang assumed that the volume of the material transport from the grain boundary to a pore is affected by the surface area of the pore. For lattice diffusion, the densification rate is written as:[51][53]

$$\frac{d\rho}{dt} = \frac{441 D_L \gamma_S V_m}{RTG^3}(1-\rho)^{1/3} \quad (31)$$

Integrating Eq. (31)

$$G^3 = \frac{k_3}{T(1-\rho)^{2/3}} t \quad (32)$$

where D_L is the lattice diffusion coefficient, γ_S is specific surface energy, V_m is the molar volume, G is grain size, ρ is relative density, t is time, T is the absolute temperature and k_3 is a constant related to the material and grain growth mechanism.

In the case of grain boundary diffusion, the densification rate is expressed as:

$$\frac{d\rho}{dt} = \frac{773 D_b \delta_b \gamma_S V_m}{RTG^4} \quad (33)$$

Integrating Eq. (33)

$$G^4 = \frac{k_4}{T\rho} t \quad (34)$$

where D_b is the grain boundary diffusion coefficient, δ_b is the diffusion thickness of grain boundary diffusion and k_4 is a constant related to the material and grain growth mechanism.

In the case of surface diffusion, the densification rate is the same as Coble's model. Fittings of the experimental results plotted according to the Eq. (33) and (34) are

show in Fig. 41. The grain growth mechanism was identified by comparing the correlation coefficient R^2. A correlation coefficient of 1 would be an ideal fit to the corresponding mechanism. It can be seen that a correlation coefficient close to 1, and thus a good linear fit was observed for the lattice diffusion controlled grain growth when sintering for 360mins and grain boundary diffusion controlled grain growth when sintering for 90mins.

Experimental on grain growth and densification kinetic of the microstructure shows that for 316L stainless steel 15μm sintering 90mins, the surface diffusion controlled pore dragged grain boundary migration and grain boundary diffusion controlled the grain growth kinetic. On the other hand, for sintering 360mins, lattice diffusion controlled the pore dragged grain boundary migration and lattice diffusion controlled the grain growth kinetic.

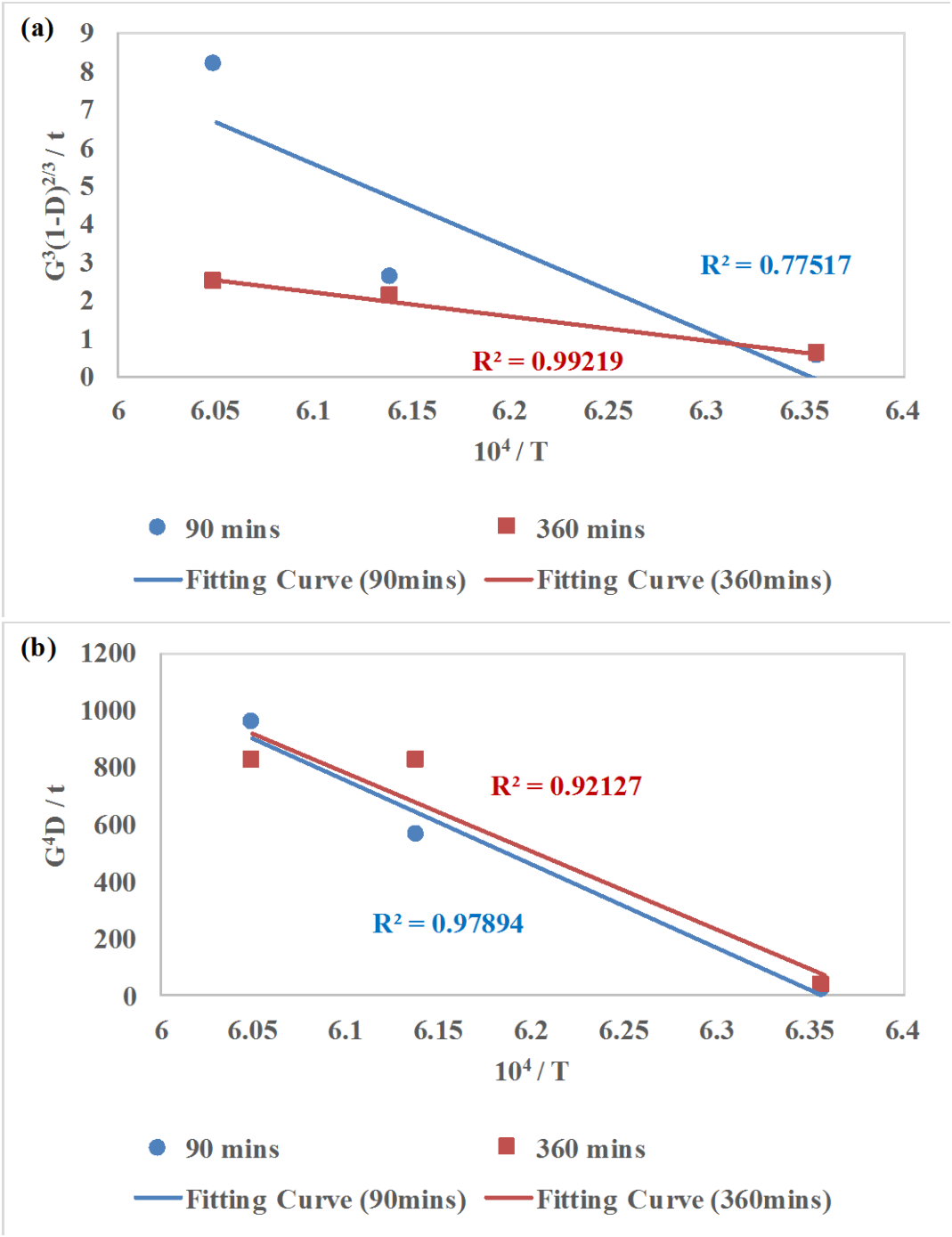

Fig. 41. 316L stainless steel 15µm grain growth data of microstructure fitted according to: (a) Kang's model of lattice diffusion controlled densification and (b) Kang's model of grain boundary diffusion controlled densification.

The experimental data works on densification and grain growth, shows that Coble's model for grain growth and Kang's model for densification all fits good for the results. For the 90mins, the grain boundary diffusion controlled grain growth and pore migration. For the 360mins, the lattice diffusion controlled grain growth and pore migration.

5.4 EFFECT OF SINTERING ATMOSPHERE

Sintering in a vacuum system can eliminate the pore gas pressure effect, giving rapid and complete densification.[18] From Table. 5. and Fig. 42., in a vacuum system leads 10% higher densification than in argon system when sintering at same temperature (1300 ºC). Compare the particle size effect, vacuum system has the same result as argon system that 15μm particle size has the highest density, as shows in Fig. 42.

Table. 5. Densification of sintering at 1300 ºC for 90mins in different atmosphere with different particle size.

Densification	Atmosphere	
Particle size (μm)	Vacuum	Argon
41	80.86%	68.41%
24	84.63%	69.13%
15	88.14%	73.41%

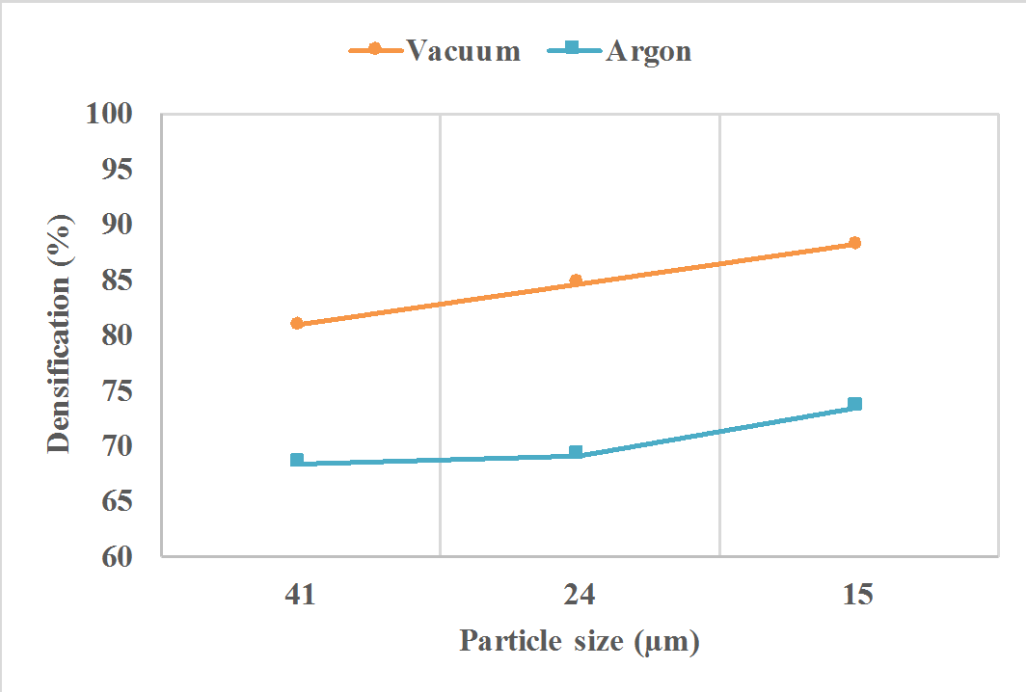

Fig. 42. Comparison of vacuum and argon atmosphere influencing the densification with different particle size.

Fig. 43. show the microstructure of sintering in different atmosphere. Fig. 43. (a)-(c) are sintering in vacuum system the pore area is less than Fig. 43. (d)-(f) which sintering in argon gas system. The size and number of pores of the part which is sintering in vacuum are smaller than sintering in argon. Since no gas is trapped in the

pores during sintering in vacuum, a higher density can be obtained. At this same lower temperature (1300 ºC), there are small amount of twin boundaries appeared when in vacuum.

Fig. 43. (d)-(f) are sintering in argon gas, pores area is bigger and form a channel along the grain boundary. The channel of pores retarded grain form, the shape of grain are mostly irregular and grain boundaries are unclear. As the previous study[54], sintering in argon will trap gas inside the pores, slow the rate of pore shrinkage and this will hinder densification.

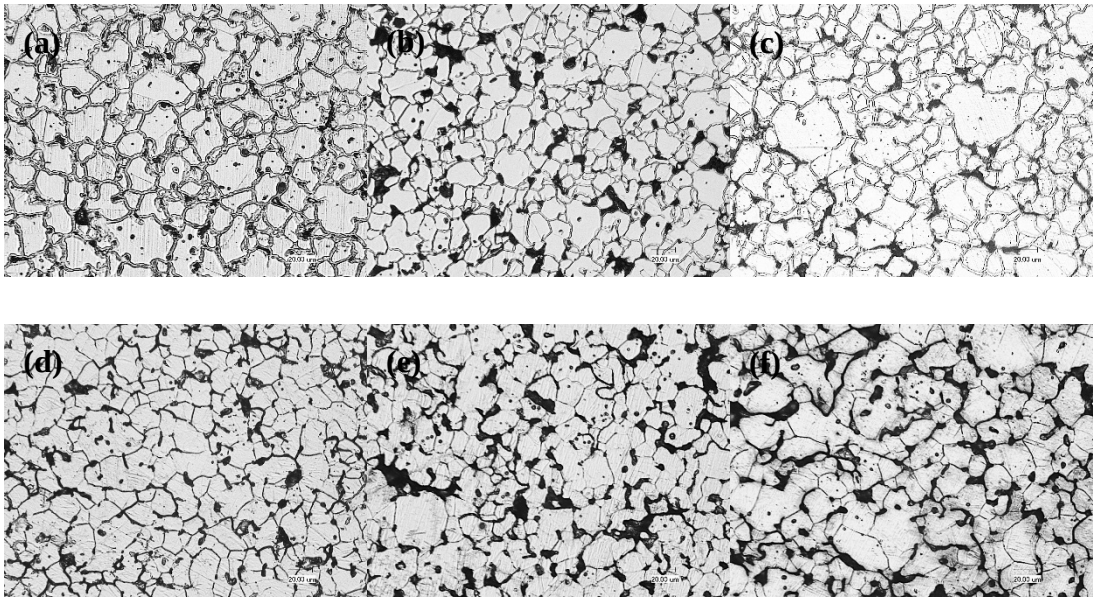

Fig. 43. Optical micrographs of the 316L stainless steel sintering at 1300 ºC for 90 mins in different atmosphere (a-c) vacuum and (d-f) argon; with different particle size (a) 15μm, (b)24μm, (c)41μm, (d)15μm, (e)24μm and (f)41μm.

6.0 CONCLUSIONS

This study investigated the variables of sintering. Four variables (particle size, sintering temperature, holding time at sintering temperature and sintering atmosphere) were designed to achieve the full density. The conclusions from the study can be summarized in several points:

1. The particle size 15μm showed the best densification after sintering. Since finer particle has initially smaller pore size which shrink easily. Both argon system and vacuum system exhibited this phenomenon.
2. The highest densification achieved was 93.90% in this study when 316L stainless steel sintering at 1356 ºC for 360 mins. However, 1356 ºC is too high according to the results. Since densification is limit at 1356 ºC even increase holding time, the best sintering temperature for this method need to set between 1300ºC and 1356ºC.
3. Grain boundary diffusion plays an important role during the sintering process. If the pore and boundary separated means the grain boundary mobility is too fast

which was correspond to the temperature is too high. Since the separation of pore-boundary will prevent the full density. For this purpose, it needs to control the grain boundary mobility and the rate of grain growth. In addition, find the appropriate sintering temperature and prolong the holding time will achieve the full densification.

4. Beside pore migration control, pore size and shape control also very important. In this research, pore from irregular shape to spherical shape when increase the sintering temperature. In fact, temperature is an important factor to control the pore shape. On the other hand, pore size generally decrease when increase the temperature; and decrease or remain stable when increase the holing time. Normally, small pores coalescence together into large pore, thus increase pore size and decrease pore numbers will cause densification increase. However, due to the entrapped gas in closed pore, the pore coarsening without the number decrease when prolonged the holding time.

Sintering in the argon gas cause the gas entrapped in the closed pore which increase the pressure in the pore and prevent the pore shrinkage. Then, sintering in the vacuum condition may reach the full density easier than sintering in the argon gas. At

same temperature and same holding time, sintering in vacuum reach higher densification than sintering in argon. Additionally, it can be predicted that full density condition can be reached at lower temperature and less holding time.

7.0 FUTURE WORK

In this study, the effect of sintering varies on sintering behavior are being investigated. Additional works need to be done to continue developing the best sintering condition to reach the full density for 316L stainless steel.

In order to get higher densification, the sintering temperature needs between 1300 ºC and 1356 ºC. Since the densification stop at 1356 ºC when increasing the temperature. Another factor of sintering is time, holding time need to extend at 1300 ºC. Due to the densification is still increasing during the prolong sintering time.

Also, controlled atmospheres that prevent the pore trapped gas. Sintering in vacuum system is a worth try for reaching full density. However, the present system can not sinter in vacuum condition higher than 1320 ºC due to the quartz tube will collapse. Therefore, build a new vacuum system with a sealed chamber which can afford high temperature and a pumping mechanism continuously extracting evolved vapors is needed.

BIBLOGRAPHY

[1] I. Gibson, D. Rosen and B. Stucker, Additive Manufacturing Technologies: 3D Printing, Rapid Prototyping and Direct Digital Manufacturing. Spring New York, 2nd edition, 2015.

[2] Y. Zhou, S.C. Siw, C. Schade, M. Chyu and C.I. Garcia, Development and Optimization for Metallic Parts/Components Using Powder Bed Additive Manufacturing, Materials Science & Technology, pp. 175-218, 2015.

[3]Erhard Klar and Prasan K. Samal, Powder metallurgy stainless steels: processing, microstructures and properties, ASM International, pp.23-37, 2007.

[4]R.P. Koseski, P. Suri, N.B. Earhardt, R.M. German and Y.S. Kwon, Microstructural evolution of injection molded gas- and water-atomized 316L stainless steel powder during sintering, Materials Science and Engineering A, vol. 402, pp. 171-177, 2005.

[5] R.M. German and A. Bose, Injection molding of metals and ceramics, Metal Powder Industries Federation, pp. 67-74, 1997.

[6] Y. Zhou, S.C. Siw, C. Schade, M. Chyu and C.I. Garcia, Development and optimization for metallic parts/components using powder bed additive manufacturing, Materials Science & Technology, 2015.

[7] H. Chen and Y.F. Zhao, Process parameters optimization for improving surface quality and manufacturing accuracy of binder jetting additive manufacturing process, Rapid Prototyping Journal, vol. 22, pp. 527-538, 2016.

[8]S. Shrestha and M. Guha, Optimization of binder jetting using Taguchi method, JOM, vol. 69, pp.491-497, 2017.

[9] R.M. German, Sintering Theory and Practice, John Wiley & Sons, Inc. 1996.

[10] Suk-Joong L. Kang. Sintering: Densification, grain growth and microstructure, Elsevier, 2005.

[11] F. Thummler and R. Oberacker, Introduction to powder metallurgy, The Institute of Materials Series on Powder Metallurgy, 1993.

[12] R.M. German, Powder metallurgy science, Metal Powder Industries Federation, 1984.

[13] K. J. Yoon, and S.J.L. Kang, Densification of ceramics containing entrapped gases pressure sintering, Journal of the European Ceramic Society, vol.6, pp201-02, 1990.

[14] R.M. German, Powder Metallurgy Science, Metal Powder Industries Federation, 1989.

[15] T. Senda and R.C. Bradt, Grain growth of zinc oxide during the sintering of zinc oxide-antimony oxide ceramics, Journal of the American Ceramic Society, vol.74, pp.1296-1302, 1991.

[16] R.M. German, Coarsening in sintering: Grain shape distribution, grain size distribution, and grain growth kinetics in solid-pore systems, Solid State and Materials Sciences, vol.35, pp. 263-305, 2010.

[17] A. Bose and R.M. German, Sintering atmosphere effects on tensile properties of heavy alloys, Metallurgical Transactions A, vol.19, pp.1467-1476, 1988.

[18] R.M. German and K.S. Churn, Sintering atmosphere effects on the ductility of W-Ni-Fe heavy metals, Metallurgical Transactions A, vol.15, pp.747-754, 1984.

[19] G.L. Powell, Mass spectrometric determination of hydrogen thermally evolved from tungsten-nickel-iron alloys, Analytical Chemistry, vol.44, pp.2357-2361, 1972.

[20] C. Toennes, R.M. German. Density and microstructure control in a martensitic stainless steel through enhanced sintering, Powder Metallurgy, vol.24, pp.151-157, 1992.

[21] R. M. German, P. Suri and S.J. Park, Review: liquid phase sintering, Journal of Material Science, vol.44, pp.1-39, 2009.

[22] Seong-Jai Cho, Suk-Joong L. and Duk N. Yoon, Effect of entrapped inert gas on pore filling during liquid sintering, Metallurgical Transactions A, vol.17, pp.2175-2182, 1986.

[23] S.J. Cho, S.J. Kang and D.N. Yoon, Effect of entrapped inert gas on pore filling during liquid phase sintering, Metallurgical Transactions A, vol. 17, pp.2175-2182, 1986.

[24] A.J. Markworth, On the volume-diffusion-controlled final stage densification of a porous solid, Scripta Metallurgica, vol.6, pp.957-960, 1972.

[25] K.S. Churn and D.N. Yoon, Pore formation and its effect on mechanical properties in W-Ni-Fe heavy alloy, Powder Metallurgy, vol.4, pp.175-178, 1979.

[26] U.C. OH, Y.S. Chung, D.Y. Kim and D.N. Yoon, Effect of grain growth on pore coalescence during the liquid-phase sintering of MgO-$CaMgSiO_4$ systems, Journal of the American Ceramic Society, vol.71, pp. 854-857, 1988.

[27] A.P. Greenough, Grain boundaries and sintering, nature, vol. 166, pp.904-905, 1950.

[28] W.D. Kingery and B. Francois, The Sintering of crystalline oxides. I. Interactions between grain boundaries and pores, Sintering and Related Phenomena, pp. 471-498, 1967.

[29] R.J. Brook, Controlled grain growth, Treatise on materials science and technology, vol. 9, pp.331-364, 1976.

[30] R.J. Brook, Pore-grain boundary interactions and grain growth, Journal of the American Ceramic Society, vol. 52, pp.56-57, 1969.

[31] O. Blaschko, R. Glas, G. Krexner and P. Weinzierl, Stage of surface and pore volume evolution during sintering, Acta metallurgica, vol. 42, pp. 43-50, 1994.

[32] M. Sakarcan, C.H. Hsueh and A.G. Evans, Experimental assessment of pore breakaway during sintering, Journal of the American Ceramic Society, vol. 66, pp. 456-461, 1983.

[33] J. Brett and L. Seigle, Shrinkage of voids in copper, Acta Metallurgica, vol.11, pp. 467-474, 1963.

[34] Erhard Klar and Prasan Samal. Powder Metallurgy Stainless steels. ASM International. pp.15, 2007.

[35] ExOne Digital Part Materialization, Idea to printed part in record time, http://www.exone.com, the ExOne company, 2015.

[36] Y. Zhou, S.C. Siw, C. Schade, M. Chyu and C.I. Garcia, Development and optimization for metallic parts/components using powder bed additive manufacturing, Materials Science & Technology, 2015.

[37] ASTM Standard B962-15: Standard Test Methods for Density of Compacted or Sintered Powder Metallurgy (PM) Products Using Archimedes' Principle, ASTM International, West Conshohocken, 2015.

[38] A. B. Spierings, M. Schneider and R. Eggenberger. Comparison of density measurement techniques for additive manufactured metallic parts. Rapid Prototyping Journal, 17(5), pp380-386, 2011.

[39] ASTM Standard E112-88: Standard Test Method for Determining Average Grain Size, 1995 Annual Book of ASTM Standards, Section 3, vol. 3.01.

[40] B.B. Mandelbrot, The fractal geometry of nature, 1st ed, New York: W.H. Freeman & Company, 1982.

[41] H.P. Tang, J.Z. Wang, J.L. Zhu, Q.B. Ao, J.Y. Wang, B.J. Yang and Y.N. Li, Fractal dimension of pore-structure of porous metal materials made by stainless steel powder, vol. 217, pp. 383-387, 2012.

[42] L.T. Dougan and P.S. Addison, Estimating the cut-odd in fractal scaling of fractured concrete, Cement and Concrete Research, vol. 31, pp. 1043-1048, 2001.

[43] Y.Shi, X.P. Lou and S.H. Quan, Fractal dimension computation methods for gas diffusion layer of PEM fuel cells, Journal of Wuhan University of Technology, vol. 29, pp. 79-82, 2005.

[44] F.K. Yan, G.Z. Liu, N.R. Tao and K.Lu, Strength and ductility of 316L austenitic stainless steel strengthened by nano-scale twin bundles, Acta Materialia, vol. 60, pp. 1059-1071, 2012.

[45] J.R. Cahoon, Q.Li and N.L. Richards, Microstructural and processing factors influencing the formation of annealing twins, Materials Science and Engineering: A, vol. 526, pp. 56-61, 2009.

[46] K.H. Song, Y.B. Chun and S.K. Hwang, Materials Science and Engineering: A, vol. 454-455, pp.629-636, 2007.

[47] J. Kong, C. Xu, J. Li, W. Chen and H. Hou, Evolution of fractal features of pores in compacting and sintering process, Advanced Powder Technology, vol. 22, pp. 439-442, 2011.

[48] R.M. German, Powder injection molding, Metal Powder Industries Federation, 1990.

[49] R.L. Coble, Sintering crystalline solids. I. Intermediate and final state diffusion models, Journal of Applied Physics, vol. 32, pp. 787-792, 1961.

[50] A. Dias, N.D.S. Mohallem and R.L. Moreira, Solid-state sintering of hydrothermal powders: Densification and grain growth kinetics of nickel-zinc ferrites, vol. 33, pp.475-486, 1998.

[51] L. Liu, N.H. Loh, B.Y. Tay, S.B. Tor, Y. Murakoshi and R. Maeda, Densification and grain growth of stainless steel microsize structure fabricated by μMIM, Applied Physics A: Materials Science & Processing, vol. 83, pp. 31-36, 2006.

[52] L.Liu, N.H. Loh, B.Y. Tay, S.B. Tor, Y. Murakoshi and R. Maeda, Micro powder injection molding: Sintering kinetics of microstructured components, Scripta Materialia, vol. 55, pp. 1103-1106, 2006.

[53] S.J.L. Kang and Y.I Jung, Sintering kinetics at final stage sintering: model calculation and map construction, Acta Materialia, vol. 52, pp. 4573-4578, 2004.

[54] C.H. Ji, N.H. Loh, K.A. Khor, S.B. Tor, Sintering study of 316L stainless steel metal injection molding part using Taguchi method: final density, Materials Science and Engineering A, vol. 311, pp. 74-82, 2001.